Fig. 4. Effects of adiponectin on MC3T3-E1 osteoblasts. (A) ALP mRNAs in MC3T3-E1 cells treated with or without adiponectin for 12 or 18 days were measured by real-time quantitative reverse transcriptase-PCR as described in Materials and methods. Data are normalized with 18S RNAs and expressed as means ± SEM of three independent experiments. $^{**}P < 0.01$, compared with the control. (B) The mineralization activity of MC3T3-E1 cells treated with or without adiponectin for 12 or 18 days was measured as described in Materials and methods. Data are expressed as means ± SEM of three independent experiments. $^{**}P < 0.01$, compared with the control.

effect on plasma glucose and insulin levels under control diet, although when adiponectin-KO mice are fed with high fat diet, their plasma glucose and insulin levels significantly elevate compared to wild-type mice and adiponectin-adenovirus reverses them to the level of wild-type mice [19]. Therefore, this effect of adiponectin should not be mediated by its systemic insulin-sensitizing effect in normal mice. However, whether it is mediated by local insulin-sensitizing effect remains to be elucidated.

The bone-forming activity of osteoblasts is also important in determining bone mass [37,38]. Our study revealed that adiponectin increased mRNA expression of ALP and mineralization activity of mouse MC3T3-E1 osteoblasts. We also investigated the effect of adiponectin on the osteoblastogenesis of primary mouse osteoblasts and mouse bone marrow cells. However, the effect was not significant on these cells (data not shown), indicating that adiponectin may have the potential to activate osteoblasts, but its effect may be dependent on the cell types.

In conclusion, we have demonstrated in the present study that adiponectin increases bone mass by suppressing osteoclastogenesis and possibly by activating osteoblastogenesis. These results suggest that increasing the concentration and/or enhancing the activity of adiponectin might be therapeutically beneficial for patients with reduced bone mass.

Acknowledgments

We are grateful to F. Ikeda, R. Nishimura, T. Yoneda, and K. Sudo for the excellent technical assistance. We thank all members of Shimomura's laboratory for the helpful discussion and comments. This study was supported in part by Yamanouchi Pharmaceutical Co., Ltd., Suzuken Memorial Foundation, The Tokyo Biochemical Research Foundation, Takeda Medical Research Foundation, Uehara Memorial Foundation, Takeda Science Foundation, Novartis Foundation (Japan) for the Promotion of Science, The Cell Science Research Foundation, The Mochida Memorial Foundation for Medical and Pharmaceutical Research, Grant-in-Aid from the Japan Medical Association, The Naito Foundation, a grant from the Japan Heart Foundation Research, Kato Memorial Bioscience Foundation, Japan Research Foundation for Clinical Pharmacology, The 21st Century COE Program, Japan, grants from the Ministry of Health, Labour and Welfare, Japan, and grants from the Ministry of Education, Culture, Sports, Science and Technology, Japan.

Appendix A. Supplementary data

Supplementary data associated with this article can be found, in the online version, at doi:10.1016/j.bbrc.2005.03.210.

References

[1] D.M. Smith, M.R. Khairi, C.C. Johnston Jr., The loss of bone mineral with aging and its relationship to risk of fracture, J. Clin. Invest. 56 (1975) 311–318.
[2] B.L. Riggs, L.J. Melton, Involutional osteoporosis, N. Engl. J. Med. 314 (1986) 1676–1686.
[3] M.F. Pittenger, A.M. Mackay, S.C. Beck, R.K. Jaiswal, R. Douglas, J.D. Mosca, M.A. Moorman, D.W. Simonetti, S. Craig, D.R. Marshak, Multilineage potential of adult human mesenchymal stem cells, Science 284 (1999) 143–147.
[4] J.E. Dennis, A. Merriam, A. Awadallah, J.U. Yoo, B. Johnstone, A.I. Caplan, A quadripotential mesenchymal progenitor cell isolated from the marrow of an adult mouse, J. Bone Miner. Res. 14 (1999) 700–709.
[5] I. Shimomura, T. Funahashi, M. Takahashi, K. Maeda, K. Kotani, T. Nakamura, S. Yamashita, M. Miura, Y. Fukuda, K. Takemura, K. Tokunaga, Y. Matsuzawa, Enhanced expression of PAI-1 in visceral fat: possible contributor to vascular disease in obesity, Nat. Med. 2 (1996) 800–803.
[6] G.S. Hotamisligil, N.S. Shargill, B.M. Spiegelman, Adipose expression of tumor necrosis factor-alpha: direct role in obesity-linked insulin resistance, Science 259 (1993) 87–91.
[7] C.M. Steppan, S.T. Bailey, S. Bhat, E.J. Brown, R.R. Banerjee, C.M. Wright, H.R. Patel, R.S. Ahima, M.A. Lazar, The hormone resistin links obesity to diabetes, Nature 409 (2001) 307–312.
[8] J.M. Friedman, J.L. Halaas, Leptin and the regulation of body weight in mammals, Nature 395 (1998) 763–770.
[9] P. Laharrague, D. Larrouy, A.M. Fontanilles, N. Truel, A. Campfield, R. Tenenbaum, J. Galitzky, J.X. Corberand,

L. Penicaud, L. Casteilla, High expression of leptin by human bone marrow adipocytes in primary culture, FASEB J. 12 (1998) 747–752.
[10] T. Thomas, F. Gori, S. Khosla, M.D. Jensen, B. Burguera, B.L. Riggs, Leptin acts on human marrow stromal cells to enhance differentiation to osteoblasts and to inhibit differentiation to adipocytes, Endocrinology 140 (1999) 1630–1638.
[11] B. Burguera, L.C. Hofbauer, T. Thomas, F. Gori, G.L. Evans, S. Khosla, B.L. Riggs, R.T. Turner, Leptin reduces ovariectomy-induced bone loss in rats, Endocrinology 142 (2001) 3546–3553.
[12] C.M. Steppan, D.T. Crawford, K.L. Chidsey-Frink, H. Ke, A.G. Swick, Leptin is a potent stimulator of bone growth in ob/ob mice, Regul. Pept. 92 (2000) 73–78.
[13] P. Ducy, M. Amling, S. Takeda, M. Priemel, A.F. Schilling, F.T. Beil, J. Shen, C. Vinson, J.M. Rueger, G. Karsenty, Leptin inhibits bone formation through a hypothalamic relay: a central control of bone mass, Cell 100 (2000) 197–207.
[14] K. Maeda, K. Okubo, I. Shimomura, T. Funahashi, Y. Matsuzawa, K. Matsubara, cDNA cloning and expression of a novel adipose specific collagen-like factor, apM1 (AdiPose Most abundant Gene transcript 1), Biochem. Biophys. Res. Commun. 221 (1996) 286–289.
[15] P.E. Scherer, S. Williams, M. Fogliano, G. Baldini, H.F. Lodish, A novel serum protein similar to C1q, produced exclusively in adipocytes, J. Biol. Chem. 270 (1995) 26746–26749.
[16] E. Hu, P. Liang, B.M. Spiegelman, AdipoQ is a novel adipose-specific gene dysregulated in obesity, J. Biol. Chem. 271 (1996) 10697–10703.
[17] T. Yamauchi, J. Kamon, H. Waki, Y. Terauchi, N. Kubota, K. Hara, Y. Mori, T. Ide, K. Murakami, N. Tsuboyama-Kasaoka, O. Ezaki, Y. Akanuma, O. Gavrilova, C. Vinson, M.L. Reitman, H. Kagechika, K. Shudo, M. Yoda, Y. Nakano, K. Tobe, R. Nagai, S. Kimura, M. Tomita, P. Froguel, T. Kadowaki, The fat-derived hormone adiponectin reverses insulin resistance associated with both lipoatrophy and obesity, Nat. Med. 7 (2001) 941–946.
[18] A.H. Berg, T.P. Combs, X. Du, M. Brownlee, P.E. Scherer, The adipocyte-secreted protein Acrp30 enhances hepatic insulin action, Nat. Med. 7 (2001) 947–953.
[19] N. Maeda, I. Shimomura, K. Kishida, H. Nishizawa, M. Matsuda, H. Nagaretani, N. Furuyama, H. Kondo, M. Taka hashi, Y. Arita, R. Komuro, N. Ouchi, S. Kihara, Y. Tochino, K. Okutomi, M. Horie, S. Takeda, T. Aoyama, T. Funahashi, Y. Matsuzawa, Diet-induced insulin resistance in mice lacking adiponectin/ACRP30, Nat. Med. 8 (2002) 731–737.
[20] T. Yamauchi, J. Kamon, Y. Minokoshi, Y. Ito, H. Waki, S. Uchida, S. Yamashita, M. Noda, S. Kita, K. Ueki, K. Eto, Y. Akanuma, P. Froguel, F. Foufelle, P. Ferre, D. Carling, S. Kimura, R. Nagai, B.B. Kahn, T. Kadowaki, Adiponectin stimulates glucose utilization and fatty-acid oxidation by activating AMP-activated protein kinase, Nat. Med. 8 (2002) 1288–1295.
[21] P.A. Jansson, F. Pellme, A. Hammarstedt, M. Sandqvist, H. Brekke, K. Caidahl, M. Forsberg, R. Volkmann, E. Carvalho, T. Funahashi, Y. Matsuzawa, O. Wiklund, X. Yang, M.R. Taskinen, U. Smith, A novel cellular marker of insulin resistance and early atherosclerosis in humans is related to impaired fat cell differentiation and low adiponectin, FASEB J. 17 (2003) 1434–1440.
[22] Y. Kamada, S. Tamura, S. Kiso, H. Matsumoto, Y. Saji, Y. Yoshida, K. Fukui, N. Maeda, H. Nishizawa, H. Nagaretani, Y. Okamoto, S. Kihara, J. Miyagawa, Y. Shinomura, T. Funahashi, Y. Matsuzawa, Enhanced carbon tetrachloride-induced liver fibrosis in mice lacking adiponectin, Gastroenterology 125 (2003) 1796–1807.
[23] E. Brakenhielm, N. Veitonmaki, R. Cao, S. Kihara, Y. Matsuzawa, B. Zhivotovsky, T. Funahashi, Y. Cao, Adiponectin-induced antiangiogenesis and antitumor activity involve caspase-mediated endothelial cell apoptosis, Proc. Natl. Acad. Sci. USA 101 (2004) 2476–2481.
[24] T. Yamauchi, J. Kamon, Y. Ito, A. Tsuchida, T. Yokomizo, S. Kita, T. Sugiyama, M. Miyagishi, K. Hara, M. Tsunoda, K. Murakami, T. Ohteki, S. Uchida, S. Takekawa, N. Waki, N.H. Tsuno, Y. Shibata, Y. Terauchi, P. Froguel, K. Tobe, S. Koyasu, K. Taira, T. Kitamura, T. Shimizu, R. Nagai, T. Kadowaki, Cloning of adiponectin receptors that mediate antidiabetic metabolic effects, Nature 423 (2003) 762–769.
[25] H. Staiger, S. Kaltenbach, K. Staiger, N. Stefan, A. Fritsche, A. Guirguis, C. Peterfi, M. Weisser, F. Machicao, M. Stumvoll, H.U. Haring, Expression of adiponectin receptor mRNA in human skeletal muscle cells is related to in vivo parameters of glucose and lipid metabolism, Diabetes 53 (2004) 2195–2201.
[26] G. Chinetti, C. Zawadski, J.C. Fruchart, B. Staels, Expression of adiponectin receptors in human macrophages and regulation by agonists of the nuclear receptors PPARalpha, PPARgamma, and LXR, Biochem. Biophys. Res. Commun. 314 (2004) 151–158.
[27] M. Matsuda, I. Shimomura, M. Sata, Y. Arita, M. Nishida, N. Maeda, M. Kumada, Y. Okamoto, H. Nagaretani, H. Nishizawa, K. Kishida, R. Komuro, N. Ouchi, S. Kihara, R. Nagai, T. Funahashi, Y. Matsuzawa, Role of adiponectin in preventing vascular stenosis. The missing link of adipo-vascular axis, J. Biol. Chem. 277 (2002) 37487–37491.
[28] Y. Azuma, K. Kaji, R. Katogi, S. Takeshita, A. Kudo, Tumor necrosis factor-alpha induces differentiation of and bone resorption by osteoclasts, J. Biol. Chem. 275 (2000) 4858–4864.
[29] H. Yasuda, N. Shima, N. Nakagawa, K. Yamaguchi, M. Kinosaki, S. Mochizuki, A. Tomoyasu, K. Yano, M. Goto, A. Murakami, E. Tsuda, T. Morinaga, K. Higashio, N. Udagawa, N. Takahashi, T. Suda, Osteoclast differentiation factor is a ligand for osteoprotegerin/osteoclastogenesis-inhibitory factor and is identical to TRANCE/RANKL, Proc. Natl. Acad. Sci. USA 95 (1998) 3597–3602.
[30] G.C. Nicholson, M. Malakellis, F.M. Collier, P.U. Cameron, W.R. Holloway, T.J. Gough, C. Gregorio-King, M.A. Kirkland, D.E. Myers, Induction of osteoclasts from CD14-positive human peripheral blood mononuclear cells by receptor activator of nuclear factor kappaB ligand (RANKL), Clin. Sci. Lond. 99 (2000) 133–140.
[31] Y. Arita, S. Kihara, N. Ouchi, M. Takahashi, K. Maeda, J. Miyagawa, K. Hotta, I. Shimomura, T. Nakamura, K. Miyaoka, H. Kuriyama, M. Nishida, S. Yamashita, K. Okubo, K. Matsubara, M. Muraguchi, Y. Ohmoto, T. Funahashi, Y. Matsuzawa, Paradoxical decrease of an adipose-specific protein, adiponectin, in obesity, Biochem. Biophys. Res. Commun. 257 (1999) 79–83.
[32] M. Iwaki, M. Matsuda, N. Maeda, T. Funahashi, Y. Matsuzawa, M. Makishima, I. Shimomura, Induction of adiponectin, a fat-derived antidiabetic and antiatherogenic factor, by nuclear receptors, Diabetes 52 (2003) 1655–1663.
[33] T. Maeda, A. Matsunuma, T. Kawane, N. Horiuchi, Simvastatin promotes osteoblast differentiation and mineralization in MC3T3-E1 cells, Biochem. Biophys. Res. Commun. 280 (2001) 874–877.
[34] T. Tsurukai, N. Udagawa, K. Matsuzaki, N. Takahashi, T. Suda, Roles of macrophage-colony stimulating factor and osteoclast differentiation factor in osteoclastogenesis, J. Bone Miner. Metab. 18 (2000) 177–184.
[35] S. Takeshita, K. Kaji, A. Kudo, Identification and characterization of the new osteoclast progenitor with macrophage phenotypes being able to differentiate into mature osteoclasts, J. Bone Miner. Res. 15 (2000) 1477–1488.
[36] R.T. Franceschi, B.S. Iyer, Relationship between collagen synthesis and expression of the osteoblast phenotype in MC3T3-E1 cells, J. Bone Miner. Res. 7 (1992) 235–246.
[37] J.A. Buckwalter, R.R. Cooper, Bone structure and function, Instr. Course Lect. 36 (1987) 27–48.
[38] T. Katagiri, N. Takahashi, Regulatory mechanisms of osteoblast and osteoclast differentiation, Oral Dis. 8 (2002) 147–159.

OsteoArthritis and Cartilage (2005) **13**, 405–417

doi:10.1016/j.joca.2004.12.014

Osteoarthritis and Cartilage

International Cartilage Repair Society

OA OSTEOARTHRITIS

A new biotechnology for articular cartilage repair: subchondral implantation of a composite of interconnected porous hydroxyapatite, synthetic polymer (PLA-PEG), and bone morphogenetic protein-2 (rhBMP-2)

Noriyuki Tamai M.D., Ph.D.†, Akira Myoui M.D., Ph.D.†, Makoto Hirao M.D.†, Takashi Kaito M.D.†, Takahiro Ochi M.D., Ph.D.‡, Junzo Tanaka Ph.D.§, Kunio Takaoka M.D., Ph.D.‖ and Hideki Yoshikawa M.D., Ph.D.†*

† *Department of Orthopaedic Surgery, Osaka University Graduate School of Medicine, 2-2 Yamadaoka, Suita, Osaka 565-0871, Japan*

‡ *National Hospital Organization Sagamihara National Hospital, 18-1 Sakuradai, Sagamihara, Kanagawa 228-8522, Japan*

§ *Biomaterials Center, National Institute for Materials Science, 1-1 Namiki, Tsukuba, Ibaraki 305-0044, Japan*

‖ *Department of Orthopaedic Surgery, Osaka City University Medical School, 1-4-3 Asahimachi, Abeno-ku, Osaka 545-8585, Japan*

Summary

Objective: Articular cartilage repair remains a major obstacle in tissue engineering. We recently developed a novel tool for articular cartilage repair, consisting of a triple composite of an interconnected porous hydroxyapatite (IP-CHA), recombinant human bone morphogenetic protein-2 (rhBMP-2), and a synthetic biodegradable polymer [poly-D,L-lactic acid/polyethylene glycol (PLA-PEG)] as a carrier for rhBMP-2. In the present study, we evaluated the capacity of the triple composite to induce the regeneration of articular cartilage.

Methods: Full-thickness cartilage defects were created in the trochlear groove of 52 New Zealand White rabbits. Sixteen defects were filled with the bone morphogenetic protein (BMP)/PLA–PEG/IP-CHA composite (group I), 12 with PLA–PEG/IP-CHA (group II), 12 with IP-CHA alone (group III), and 12 were left empty (group IV). The animals were killed 1, 3, and 6 weeks after surgery, and the gross appearance of the defect sites was assessed. The harvested tissues were examined radiographically and histologically.

Results: One week after implantation with the BMP/PLA–PEG/IP-CHA composite (group I), vigorous repair had occurred in the subchondral defect. It contained an agglomeration of mesenchymal cells which had migrated from the surrounding bone marrow either directly, or indirectly via the interconnecting pores of the IP-CHA scaffold. At 6 weeks, these defects were completely repaired. The regenerated cartilage manifested a hyaline-like appearance, with a mature matrix and a columnar organization of chondrocytes.

Conclusions: The triple composite of rhBMP-2, PLA-PEG, and IP-CHA promotes the repair of full-thickness articular cartilage defects within as short a period as 3 weeks in the rabbit model. Hence, this novel cell-free implant biotechnology could mark a new development in the field of articular cartilage repair.

Key words: Articular cartilage repair, Interconnected porous hydroxyapatite (IP-CHA), BMP, PLA-PEG.

Introduction

To date, the myth "once destroyed, cartilage cannot be repaired" has yet to be dispelled[1]. Mature articular cartilage cannot heal spontaneously owing to its low mitotic activity, which contrasts to the rapid rate of chondrocytic mitosis during normal cartilage growth.

Recently, several researchers have attempted to utilize culture-expanded autologous chondrocytes in combination with collagen sponges or fibrin glue to effect the repair of cartilage defects[2,3]. However, the results were either unsatisfactory or, if satisfactory, were achieved only after a lengthy wait for the regeneration of hyaline cartilage[2,4]. These poor results may reflect the characteristics of the transplantation technique, which involves the application of cartilage-derived cells to the defect[5].

Mesenchymal stem cells (MSCs) isolated from bone marrow have the ability to differentiate into chondrocytes, osteoblasts and other connective tissue cells of mesenchymal origin when cultured under appropriate *in vitro* conditions[6,7]. In an effort to exploit the pluripotentiality of MSCs, MSC-based repair strategies have been instigated in rabbits and goats, but with limited success[8,9]. Clinically,

*Address correspondence and reprint requests to: Hideki Yoshikawa. Tel: 81-6-6879-3552; Fax: 81-6-6879-3559; E-mail: yhideki@ort.med.osaka-u.ac.jp

Received 8 November 2004; revision accepted 20 December 2004.

surgical interventions, such as microfracturing, abrasion arthroplasty and osteochondral drilling, have been widely used and considered to be partially successful[10,11]. These techniques are based on the concept that intentional damage to the subchondral bone recruits MSCs to the defect, thereby promoting cartilage repair.

A potentially powerful alternative approach for cartilage regeneration is the local administration of bone morphogenetic proteins (BMPs), which are members of the transforming growth factor-β superfamily. BMPs have been shown to regulate and promote the growth and differentiation of chondrocytes, osteoblasts and MSCs[12,13]. Indeed, recombinant human bone morphogenetic protein-2 (rhBMP-2) can stimulate the *in vitro* synthesis of components of the chondrocytic matrix, such as proteoglycans and type-II collagen[14–16]. Furthermore, BMPs are known to induce the condensation of MSCs when administered *in vivo*[17–19].

Inorganic biomaterials, such as carbon fibers[20], collagen scaffolds[2,21], absorbable polymers[22,23], and hydroxyapatite[24,25], have been used for articular cartilage repair. Some success has been achieved in the repair of small osteochondral defects, but no widely accepted method exists for the complete healing of hyaline cartilage. The cause of the failure lies not in the nature of the biomaterial itself but in its structure, which is not regulated three-dimensionally.

In the present study, we attempted to combine two distinct approaches: the strong induction of subchondral bone regeneration, with a view to recruiting bone-marrow MSCs to the osteochondral defect; and the appropriate local delivery of rhBMP-2 to induce chondrocytic differentiation and to stimulate matrix production by the chondrocytes. To instigate these two approaches simultaneously, we developed a combined biomaterial, which consists of a synthetic hydroxyapatite with an interconnected porous structure (IP-CHA), and a synthetic bioabsorbable polymer, namely, PLA–PEG (poly-D,L-lactic acid–polyethylene glycol block copolymer). In this system, PLA–PEG serves as a drug-delivery carrier, which permits the ideal release of rhBMP-2 over a period of about 3 weeks[26–29]. IP-CHA is made from hydroxyapatite, which is a bioactive ceramic with osteoconductive properties[30,31]. In addition, IP-CHA has a finely organized, three-dimensional interconnecting pore structure. The material is highly porous (porosity: 75%) and the pore size (150 μm) is appropriate for bone formation. The large interconnecting channels (average diameter: 40 μm) permit the easy penetration of tissue into the deep pores[30]. Owing to these structural properties, IP-CHA can itself induce local bone repair processes[30,32,33]. The interconnecting pore structure of the material also permits its easy impregnation with cytokines or growth factors borne by an appropriate delivery system.

The rationale behind the selection of key experimental design parameters was as follows: Skeletally immature adolescent rabbits (4–6 months old and 2.5–3.0 kg in weight) were selected because the ability of articular cartilage to repair depends mostly on the bone-marrow MSCs, which are metabolically more active and have a higher capacity to induce repair in an immature model. The decision to use full-thickness defects with a diameter of 4 mm and a depth of 6 mm was based on the results of previous studies. In rabbits, partial-thickness defects do not heal spontaneously, whereas full-thickness ones with a diameter less than 3 mm do, and the repair tissue is composed either of hyaline- or of fibrocartilage[34–36]. Hence, it was necessary to establish a model in which this upper limit for spontaneous repair was exceeded.

In the present study, we demonstrate the capacity of the triple composite of rhBMP-2, PLA-PEG, and IP-CHA to effect articular cartilage repair. The goal was to achieve the repair of full-thickness articular cartilage defects in rabbits in as short a time as possible, with the ultimate view of inducing the repair of similar lesions in humans; specifically, those generated during osteoarthritis, rheumatoid arthritis, and osteochondritis dissecans.

Materials and methods

PREPARATION OF IMPLANTS

IP-CHA was synthesized by Toshiba Ceramics Co., Ltd. (Kanagawa, Japan), as previously described[30]. In short, we adopted a "foam gel" technique, which involves two unique steps: a foaming step and a crosslinking step. During the foaming step, the hydroxyapatite slurry is mixed with a foaming agent (polyethyleneimine, 40% by weight). During the crosslinking (polymerization) step, the foam-like hydroxyapatite slurry is rapidly gelatinized using a water-soluble crosslinking agent (a poly-functional epoxy compound)[30].

rhBMP-2, which is produced by the Genetics Institute (Cambridge, MA) and was given to us by Yamanouchi Pharmaceutical Co., Ltd. (Ibaraki, Japan), was dissolved in buffer (5 mM glutamic acid, 2.5% glycine, 0.5% sucrose, and 0.01% Tween 80) at a concentration of 1 mg/ml. The solution was then filter-sterilized. Two-hundred mg of PLA–PEG [molecular weight (MW) = 11,400, dispersity (Mw/Mn) = 1.1 (Taki Chemical Research Laboratory, Kanagawa, Japan)] was dissolved in 1 ml of acetone. To prepare a single implant sample, a 25 μl aliquot of the PLA–PEG mass (5 mg) was mixed with a 20 μl sample of rhBMP-2 (20 μg). The specimen of IP-CHA (4 mm in diameter and 4 mm in height) was immersed in the mixture and the solvent was evaporated in a centrifuge/evaporator. The resulting BMP/PLA–PEG/IP-CHA composite was sterilized with ethylene oxide gas for 24 h on the day preceding implantation.

IN VITRO RELEASE KINETICS OF RHBMP-2

The release of rhBMP-2 from the BMP/PLA–PEG/IP-CHA composite was measured using a quantitative sandwich enzyme immunoassay technique (AN'ALYZA®; BMP-2 immunoassay, TECHNE Co. MN, USA). The dose of rhBMP-2 used in the *in vivo* experiments (20 μg) was chosen for the release study. Twelve BMP/PLA–PEG/IP-CHA composites, which were prepared in the same way as those used for implantation in the rabbit model, were placed within 24-well plates together with 500 μl of phosphate-buffered saline [(PBS) Sigma] and incubated for 21 days at 37°C. The supernatant was removed and replaced with fresh PBS every day. The supernatants removed on days 1, 3, 7, 14 and 21 were analyzed for their concentrations of rhBMP-2 according to the enzyme-linked immunosorbent assay (ELISA) technique. The bioactivity of the composites maintained *in vitro* for 0, 7 and 21 days (four samples per time point) was also assessed (see next section).

IN VIVO BIOASSAY FOR THE BMP/PLA–PEG/IP-CHA COMPOSITE

To assess the biological activity of composites that were maintained *in vitro* for 0, 7 and 21 days, these, as well as

IP-CHAs without rhBMP-2 (controls), were implanted within the back muscles of 5-week-old male JCL: ICR mice (one composite per animal; four mice per group, i.e., control, day 1, day 7 and day 21) as previously reported[27,28]. The implants were harvested 2 weeks after implantation. They were then crushed, homogenized in 0.2% Nonidet P-40 containing 1 mM $MgCl_2$, and centrifuged at 10,000 rpm for 1 min at 4°C. The supernatants were assayed for alkaline phosphatase (ALP) activity using *p*-nitrophenyl phosphate as a substrate. The product was measured spectrophotometrically at an absorption wavelength of 410 nm ($n = 4$ per group)[37].

ANIMAL EXPERIMENTS

Fifty-two New Zealand White rabbits weighing 2.5–3.0 kg (4–6 months) were kept in cages and had free access to food pellets and water. The rabbits were anesthetized by the intravenous injection of 1 ml of pentobarbital [50 mg/ml (Nembutal®; Dainippon Pharmaceutical Co. Ltd., Osaka, Japan)] and the intramuscular injection of 1 ml of xylazine hydrochloride [25 mg/ml (Seractal®; Bayer, Germany)]. After shaving, disinfection, and draping, a straight 3-cm long medial parapatellar incision was made over the right knee and the patella was everted. Full-thickness articular osteochondral defects, 4 mm in diameter and 6 mm in depth, were created mechanically in the patellar groove of the right distal femur. Rabbit knees were divided into four implant groups: group I ($n = 16$ knees) received the BMP/PLA–PEG/IP-CHA composite; group II ($n = 12$ knees) received the PLA–PEG/IP-CHA composite (no rhBMP-2), group III ($n = 12$ knees) received IP-CHA alone; and group IV ($n = 12$ knees) underwent a sham operation with no implantation. In groups I, II, and III, all implants were placed at the subchondral bone level, 2 mm beneath the surface of the adjacent cartilage. The fascial layer was closed with absorbable sutures, and the skin with 4-0 nylon sutures. One week after surgery, four rabbits in group I were killed. At 3 weeks, 24 rabbits were killed (group I = 6, group II = 6, group III = 6, group IV = 6), and at 6 weeks 24 rabbits were killed (group I = 6, group II = 6, group III = 6, group IV = 6). The animals were killed by an intravenous injection of 5 ml of pentobarbital (Table I). All animal experiments were approved by the Animal Laboratory, Faculty of Medicine, Osaka University, Japan.

RADIOGRAPHIC AND HISTOLOGICAL EVALUATIONS

The harvested tissues were radiographed using a soft X-ray apparatus [35 kV; 300 μA; 300 s; MX20 (Faxitron X-ray Co., IL, USA)] and then fixed in 4% paraformaldehyde (pH 7.4) for 48 h at 4°C. Tissue samples were decalcified in 20% ethylenediaminetetraacetic acid (pH 7.4) at 4°C, dehydrated in a graded ethanol series and embedded in paraffin. Serial sections (5 μm in thickness) were cut sagittally through the center of the operative site and stained with hematoxylin and eosin (H&E) or with safranin-O. For the immunohistochemical analysis, paraffin sections were treated with 3% H_2O_2 to block endogenous peroxidase activity. They were pretreated with serum to block non-specific staining. The sections were then incubated with mouse monoclonal antibodies: anti-type-I collagen (I-8H5, Daiichi Fine Chemical Co., Ltd, Toyama, Japan), anti-type-II collagen (II-4C11, Daiichi Fine Chemical Co., Ltd, Toyama, Japan), and anti-CD105 [(Endoglin) 555722, BD Bioscience, NJ, USA]; and with the polyclonal antibody goat anti-Cbfa1 [(Runx2) C-19, Santa Cruz, CA, USA][38]. The specimens were treated with the appropriate biotinylated secondary antibodies, and then incubated with the streptavidin/horseradish peroxidase complex. The signal was visualized as the red reaction product of a 3-amino-9-ethyl carbazole liquid substrate chromogen (AEC, DAKO JAPAN Co., Ltd, Kyoto, Japan). To confirm the specificity of

Table I
Information respecting the deployment of the 52 rabbits used in this study

	Number of rabbits				Total number
	Group I	Group II	Group III	Group IV	
Materials					
IP-CHA	+	+	+	–	
rhBMP-2	+	–	–	–	
PLA–PEG	+	+	–	–	
Follow-up time					
1 week	4	0	0	0	4
3 weeks	6	6	6	6	24
6 weeks	6	6	6	6	24
Total number	16	12	12	12	52

Table II
*Histological scoring system**

Category	Points
Cell morphology	
Hyaline cartilage	4
Mostly hyaline cartilage	3
Mostly fibrocartilage	2
Mostly non-cartilage	1
Non-cartilage only	0
Matrix-staining (metachromasia)	
Normal	3
Slightly reduced	2
Markedly reduced	1
No metachromatic staining	0
Structural integrity	
Normal	2
Slight disruption	1
Severe disintegration	0
Surface regularity†	
Smooth	3
Moderate	2
Irregular	1
Severely irregular	0
Thickness of cartilage, %	
121–150	1
81–120	2
51–80	1
0–50	0
Regenerated subchondral bone	
Good	2
Moderate	1
Poor	0
Integration with adjacent cartilage	
Both edges integrated	2
One edge integrated	1
Neither edge integrated	0
Total maximum	18

*A modified version of the system described by Wakitani *et al.*[8].

†Total smooth area of repair cartilage compared with the entire area of the cartilaginous compartment of the defect.

the antibody under the adopted conditions and to confirm the specificity of the markers in target cells, all antibodies were tested for their reactivity in control tissues.

HISTOLOGICAL SCORING

To quantify the histological repair of articular cartilage defects, we employed a modified version of the grading scale described by Wakitani *et al.*[8]. This consists of seven categories and assigns a score ranging from 0 to 18 points (Table II). The following parameters were assessed: cell morphology (hyaline cartilage); metachromatic staining of the cartilage matrix; structural integrity of the regenerated cartilage; surface regularity of the tissue; thickness of the cartilage layer; regeneration of the subchondral bone; and integration of the tissue with adjacent cartilage.

STATISTICAL ANALYSES

Data pertaining to ALP activity were analyzed using an unpaired Student's *t* test. The histological scoring data were analyzed using the Kruskal–Wallis test, with a *post hoc* Bonferroni correction for non-parametric data.

Results

EVALUATION OF THE IMPLANTS

Scanning electron microscopy of IP-CHA samples revealed these to have a finely organized three-dimensional structure. Most of the IP-CHA pores were spherical, of similar size (approximately 100–200 μm in diameter) and uniformly interconnected via channels [10–80 μm in diameter; Fig. 1(B, C)]. Scanning electron microscopy of the BMP/PLA–PEG/IP-CHA composite revealed the BMP/PLA–PEG component to affect neither the pore size nor the interconnecting pore structure and to coat well the surface of the IP-CHA [Fig. 1(D, E)].

IN VITRO RELEASE KINETICS OF RHBMP-2 AND *IN VIVO* BIOASSAY FOR THE BMP/PLA–PEG/IP-CHA COMPOSITE

Based on ELISA, the BMP/PLA–PEG/IP-CHA composite released significant quantities of rhBMP-2 during the 21-day monitoring period [6.85 ± 1.31 μg/ml on day 1, 0.79 ± 0.22 μg/ml on day 3, 22.9 ± 0.62 ng/ml on day 7, 4.76 ± 1.13 ng/ml on day 14, and 2.71 ± 0.70 ng/ml on day 21; Fig. 2(A)].

To assess the bioactivity of the BMP/PLA–PEG/IP-CHA composites maintained *in vitro* for 0, 7 or 21 days, we implanted these, as well as IP-CHAs (control for the absence of rhBMP-2) within the back muscles of male ICR mice (a standard ectopic bone-formation model) and then analyzed the explanted material for its ALP activity. High levels of ALP activity could be detected even on day 21 [Fig. 2(B)], which accords with the rhBMP-2 release kinetics results *in vitro*.

MACROSCOPIC OBSERVATIONS OF CARTILAGE DEFECTS

Three weeks after implantation, the repaired defects in group I had a macroscopically smooth and glistening appearance and exhibited continuity with the surrounding host cartilage [Fig. 3(A)]. The controls (groups II–IV) revealed varying degrees of cartilage resurfacing with fibrous tissue [Fig. 3(B–D)].

At 6 weeks, the color and the glistening appearance of the repaired defects in group I were similar to those manifested by the adjacent host cartilage. The junction between the repaired tissue and the surrounding host cartilage was not clearly visible [Fig. 3(E)]. In contrast, the regenerated tissue in the control groups (groups II–IV) was

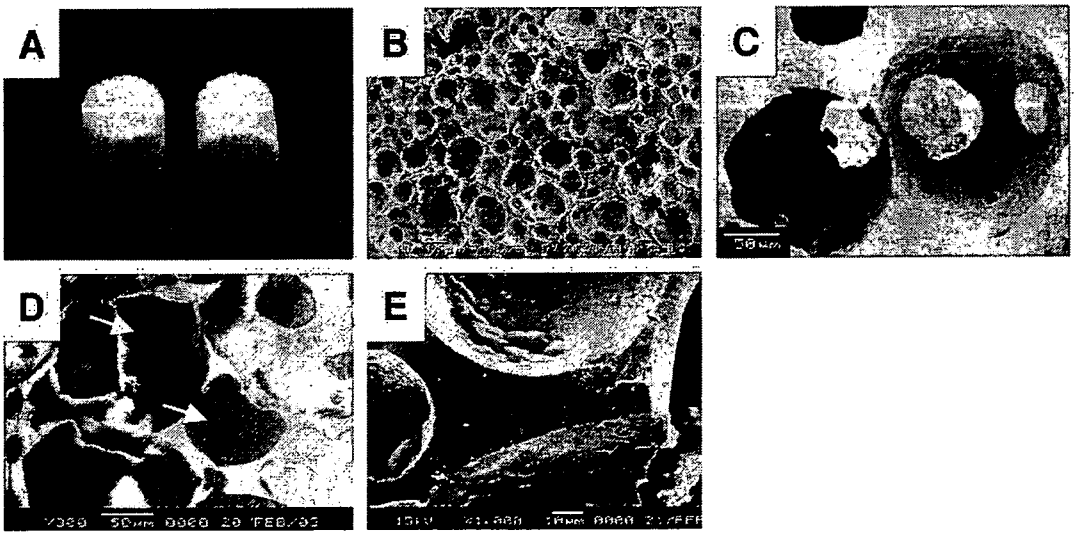

Fig. 1. Macroscopic photograph (A) and scanning electron micrographs (B–E) of IP-CHA specimens (4 mm in diameter and 4 mm in height). (A) Macroscopically, the surface of IP-CHA is slightly rough compared with that of other commercial porous hydroxyapatite materials, owing to its regular porous structure. (B, C) Scanning electron micrographs of IP-CHA, illustrating the regular arrangement of pores which are of similar size (100–200 μm in diameter), uniformly connected with each other, and separated by thin walls. (B) = 80×; (C) = 600×. (D, E) Scanning electron micrographs of the BMP/PLA–PEG/IP-CHA composite. (D) The dark areas lining the pores (white arrows) represent the BMP/PLA–PEG component. The introduction of BMP/PLA–PEG had no effect on either the pore size or the interconnecting pore structure. (E) Higher magnification of the lining of a pore (black arrow), revealing it to be well coated with BMP/PLA–PEG. (D) = 300×; (E) = 1000×.

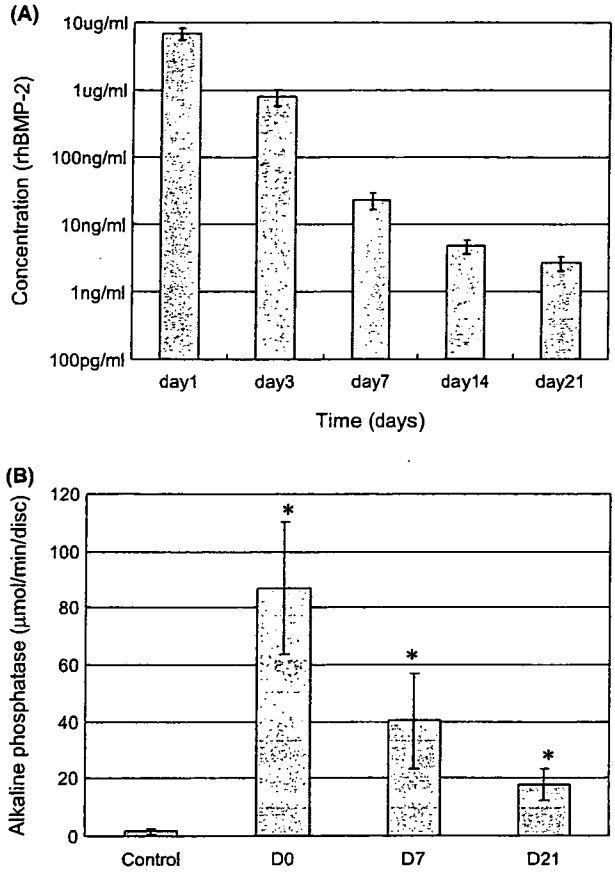

Fig. 2. Time course of rhBMP-2 release from the BMP/PLA–PEG/IP-CHA composite *in vitro* (A) and the bioactivity of the composites *in vivo* (B). (A) Release kinetics (measured by ELISA) of rhBMP-2 from the BMP/PLA–PEG/IP-CHA composite, illustrating significant quantities of rhBMP-2 during the 21-day monitoring period. The bar graph depicts the non-cumulative release at each time point. Mean values ± SD ($n = 4$) are represented. (B) The bioactivity of BMP/PLA–PEG/IP-CHA composites that were maintained *in vitro* for 0 (D0), 7 (D7), or 21 (D21) days was assessed 2 weeks after their implantation at an ectopic site in mice by monitoring the ALP activity of the explanted material. PLA–PEG/IP-CHA (no rhBMP-2) represented the control. High levels of ALP activity could be detected even on day 21 [86.8 ± 23.2 μmol/min/disc (day 0), 40.3 ± 16.8 μmol/min/disc (day 7), 17.7 ± 5.2 μmol/min/disc (day 21), 1.6 ± 0.8 μmol/min/disc (control)]. Mean values ± SD ($n = 4$) are represented. * = value is significantly different from the control ($P < 0.05$).

fibrous, and had a rough surface containing many fissures [Fig. 3(F–H)].

RADIOGRAPHIC EVALUATION

Six weeks after implantation, the soft X-ray analysis revealed defects treated with the BMP/PLA–PEG/IP-CHA composite (group I) to be consistently filled with newly formed bone, which was continuous with the surrounding intact subchondral bone [Fig. 3(I)]. In the control groups (groups II–IV), bone formation was incomplete and irregular [Fig. 3(J–L)].

HISTOLOGICAL EVALUATION

One week after implantation with the BMP/PLA–PEG/IP-CHA composite (group I), vigorous new bone formation was observed histologically within the pores of the IP-CHA scaffold [Fig. 4(B)], and about three-quarters of the defect depth above the IP-CHA had already been replaced with repair tissue. The central part of the repair tissue contained a fibrin clot and a few vessels. The lateral and lower regions consisted of granulation tissue, which was actively undergoing neovascularization and contained rounded fibroblast-like cells. These cells registered positive for Cbfa1 and/or CD105. They appeared to have infiltrated from the surrounding intact subchondral bone, either directly, or indirectly via the interconnecting IP-CHA pores, which were likewise filled with granulation tissue. Some of the pores in the peripheral 1-mm portions of IP-CHA blocks already contained newly formed bone (Fig. 4).

Three weeks after implantation with BMP/PLA–PEG/IP-CHA, the defect space above the IP-CHA blocks (subchondral space) was filled with newly generated and vigorous bone tissue, which penetrated the interconnecting pores of this material [Fig. 5(A, F)]. The regenerated articular cartilage was more cellular and contained less extracellular matrix than normal cartilage. The regenerated cartilage was divided into three distinct zones: (1) a superficial one, which contained flattened hyperchromatic cells; (2) a middle one, which contained rounded chondrocytes; and (3) a zone of enchondral ossification. The cartilage-like layer was two-to-three times thicker than normal cartilage [Fig. 5(A, E)]. In each of the control groups (groups II–IV), the regenerated fibrous cartilage had a similar morphological appearance, irrespective of the absence or presence of an implant. Although the subchondral space in group II tended to be filled with more newly formed bone than did that in the other control groups (groups III and IV), the quantitative histological evaluation revealed no significant difference between them [Table III; Fig. 5(B–D)].

Six weeks after implantation, defects treated with the BMP/PLA–PEG/IP-CHA composite (group I) were filled with regenerated subchondral bone, which also penetrated the pores of the implant. The subchondral bone was covered with a layer of regenerated cartilage tissue of almost normal thickness. The hyaline nature of the cartilage was maintained, and the tissue was beginning to assume a columnar organization and a horizontal stratification into four distinct zones (superficial, middle, deep and calcified), as in normal cartilage [Fig. 6(A, E)]. Interestingly, no gaps could be distinguished microscopically between the host cartilage and the newly regenerated cartilage, which suggests that the tissues were functionally and biologically integrated [Fig. 6(F)]. Safranin-O staining was evident predominantly in the middle and deep zones. Immunoreactivity for type-II collagen tended to be weakest in the deep zone at the junction with host tissue. But generally, the matrix exhibited a hyaline-like cartilaginous phenotype [registering negative for type-I collagen; Fig. 6(J–L)]. In contrast, defects in the control groups (groups II–IV) were filled with a hypercellular type of fibrous tissue. No hyaline cartilage was detected, despite the presence of new bone above and within the implant; [Fig. 6(B–D, G–I)]. Histological sections were assessed quantitatively using a modified version of an established grading system, which measures the degree and quality of cartilage repair[8] (Table II). At each time point, the scores for the BMP/PLA–PEG/IP-CHA composite (group I) were significantly better than those for groups II, III and IV ($P < 0.01$). These findings accord with the macroscopic and histological observations.

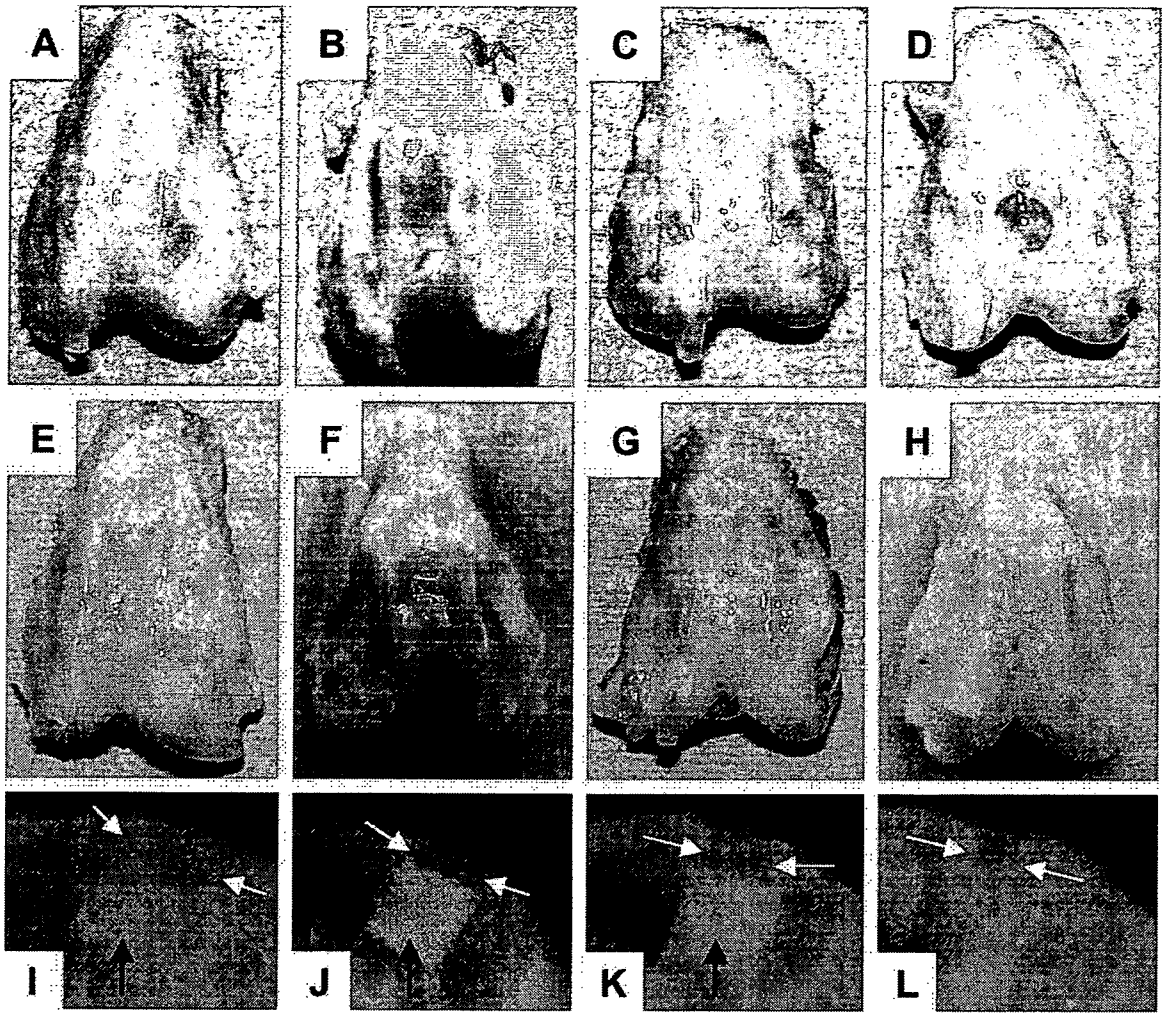

Fig. 3. Gross appearance (A–H) and soft X-ray photographs (I–L) of four specimens (one in each group) 3 weeks (A–D) and 6 weeks (E–L) after implantation. (A, E, I): BMP/PLA–PEG/IP-CHA composite (group I). (B, F, J): PLA–PEG/IP-CHA composite (group II). (C, G, K): IP-CHA alone (group III). (D, H, L): no implant (group IV). (A, E) In group I, reconstruction of the surface was good. At 3 weeks, the surface was still a little "white"; but at 6 weeks, it was smooth and glistening and exhibited continuity with the surrounding intact host cartilage. These macroscopic findings correspond with the histological results (Table III). (B, F) In group II, the articular cartilage defects were covered with "white" fibrous tissue with many fissures. (C, G) In group III, the regeneration of the defect looked better than those of other control groups (group II and IV), whereas the junction of the defects were still visible. (D, H) In group IV, in which the defects were left empty, at 3 weeks the defects were filled with red, semitransparent tissue with the margins sharply defined and the edges completely discernible (D). At 6 weeks, the defects were filled with irregular "white" tissue with pin-hole like fissure (H). (I–L) Representative soft X-ray photographs of the four specimens. The black arrows denote the implanted IP-CHA block. The white arrows above the IP-CHA block indicate the region where subchondral bone should be regenerated. A white, radiodense zone was observed above the IP-CHA block in group I (I); it denotes a vigorous regeneration of subchondral bone. This radiodense zone was not detected in groups II–IV (J–L).

Discussion

Several investigators have reported on the repair of articular cartilage defects using diverse tissue-engineering approaches. These include a gene-enhanced technique, the direct implantation of growth factors, and *in vitro* cell expansion[39–42]. BMPs have been shown to induce the differentiation of MSCs into chondrocytes both *in vitro* and *in vivo*. BMPs (BMP-2 and BMP-7) have also been used in conjunction with type-I collagen sponges to elicit the repair of osteochondral defects[43–45]. Cook *et al.*[40] have reported that type-I collagen sponges impregnated with rhBMP-7 can induce the repair of full-thickness osteochondral defects with hyaline-like cartilage in a dog model. The hyaline-like quality of the repair cartilage was still evident 52 weeks after surgery and the tissue had undergone no significant degradation. Sellers *et al.*[41] have demonstrated the capacity of rhBMP-2 to accelerate the healing of full-thickness articular cartilage defects and to improve the histological appearance and the biochemical characteristics of the repair cartilage. However, the tissue still differed from normal hyaline cartilage, both biochemically and structurally, and a long time elapsed before the defect area was completely filled with it. These suboptimal results probably reflect a limited recruitment of MSCs and/or a restricted delivery of cytokines, owing to the poor structural

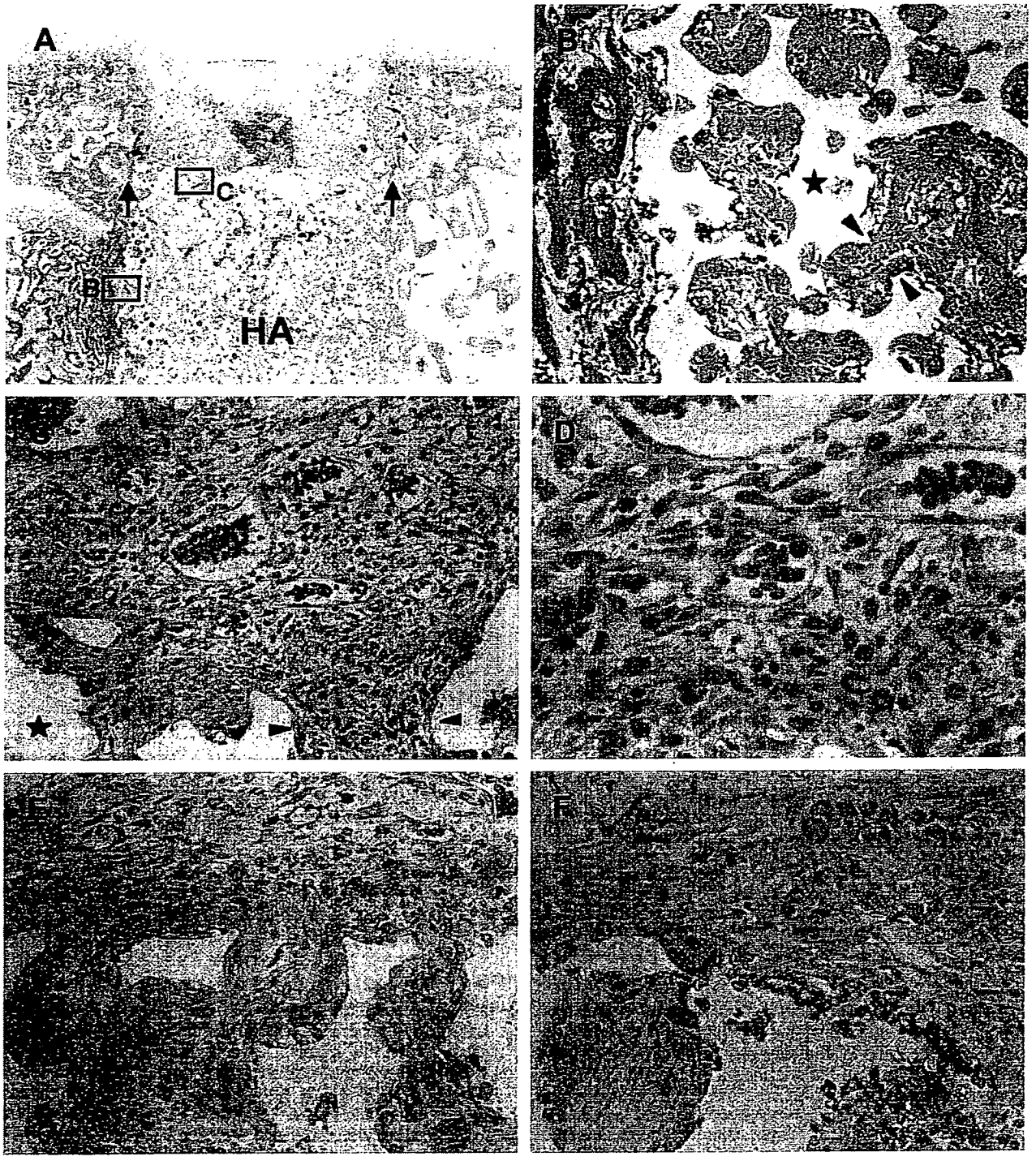

Fig. 4. Histological photomicrographs of a defect 1 week after the implantation of a BMP/PLA–PEG/IP-CHA composite (group I). (A) Overview of the defect site, the margins of which are indicated by arrows. HA represents the implanted IP-CHA scaffold (H&E). (B) Higher magnification of the region indicated in (A). The surface of newly formed bone trabeculae are lined with numerous cuboidal osteoblasts which have migrated from the neighboring host bone. (C) Higher magnification of the region indicated in (A), illustrating a neovascularized aggregate of cells which have migrated from the neighboring bone marrow, either directly or indirectly via the interconnecting channels of the IP-CHA composite. The arrowheads in (B) and (C) indicate the interconnecting pores of the IP-CHA scaffold. The asterisks denote regions that were occupied by hydroxyapatite before decalcification. (D) Higher magnification of (C), illustrating the rounded, fibroblast-like form of the aggregated cells. (E, F) Immunostaining of the aggregated cells for Cbfa1 (E) and CD105 (F). Many of the cells expressed the chondro/osteoblastic marker (E) and/or the mesenchymal one (F). Magnification: (A) = 10×; (B, C) = 100×; (E, F) = 200×; (D) = 400×.

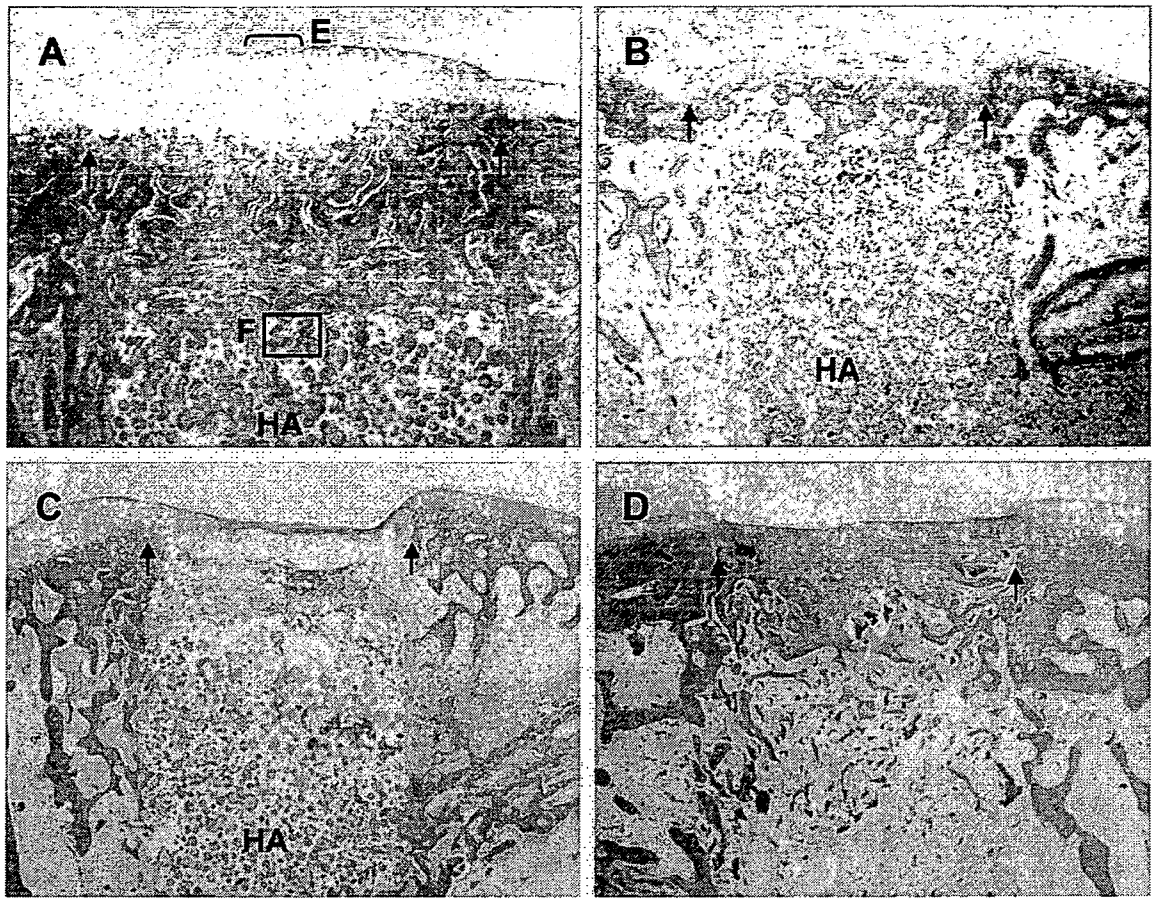

Fig. 5. Histological photomicrographs of defects (H&E staining) 3 weeks after implantation with either the BMP/PLA–PEG/IP-CHA composite [(group I) A, E, F], the PLA–PEG/IP-CHA composite [(group II) B], or IP-CHA alone [(group III) C], and in the absence of treatment [empty (group IV) D]. Arrows indicate the margins of the defect. HA represents the implanted IP-CHA scaffold. Highly magnified images of the regions indicated in (A) are represented in (E) and (F). (A) Section of a defect filled with the BMP/PLA–PEG/IP-CHA composite (group I), illustrating well-organized hyaline-like cartilage and accelerated replacement of vigorous subchondral bone. (B–D) In each of the control groups (group II–IV), the regenerated tissue had a similar morphological appearance, irrespective of the absence or presence of an implant. The defect site was filled predominantly with a hypocellular fibrocartilage repair tissue with incomplete replacement of subchondral bone. (E) The regenerated articular cartilage was more cellular and contained less extracellular matrix than normal cartilage. However, a stratified structure similar to normal cartilage was already visible. (F) Vigorous regeneration of subchondral bone occurred, which was carried up through the interconnections of the IP-CHA scaffold (arrowheads). The asterisk denotes a region that was occupied by hydroxyapatite before decalcification. Magnification: (A–D) = 10×; (E, F) = 100×.

organization of the supporting scaffold. The purpose of the present study was to evaluate the potential of IP-CHA to serve as a scaffold for the repair of full-thickness articular cartilage defects. This material has a well-organized interpore connectivity.

The osteoconductivity of polymer implants containing rhBMP-2 has been studied extensively[28,46]. In the present study, we used the synthetic bioabsorbable polymer PLA–PEG as a carrier for rhBMP-2. *In vitro*, rhBMP-2 was released continuously from the BMP/PLA–PEG/IP-CHA composite over a period of 21 days, as determined by ELISA [Fig. 2(A)]. This finding accords with the results of the *in vivo* bioassay [Fig. 2(B)], which was based on the ALP activity of composites implanted at an ectopic site in mice. However, it is of course conceivable that the release profile of rhBMP-2 at this ectopic site in mice differs greatly from that at the orthotopic site in our rabbit model.

Our new strategy for articular cartilage repair appears to be unique in three respects: (1) autogenous MSCs were efficiently recruited from the bone marrow by strongly activating regeneration within the subchondral bone compartment of the defect; (2) a sustained BMP stimulus appears to promote not only the vigorous regeneration of subchondral bone but also the ensuing differentiation of chondrocytes and the production of a cartilaginous matrix at the surface, which results in the regeneration of a hyaline-like cartilage layer in as short a time as 3 weeks; and (3) the regenerated cartilage integrated almost perfectly with the surrounding host cartilage, probably because the entire regeneration process was conducted *in situ*, i.e., it did not involve an *in vitro* chondrocyte-culturing step.

It is not known why the thickness of the repaired articular cartilage corresponded so closely to that of the host articular cartilage, with no bony differentiation. But articular factors, such as oxygen tension, joint effusion and mechanical stress, as well as subchondral influences, may regulate the differentiation process. Although the regenerated cartilage present 6 weeks after surgery was

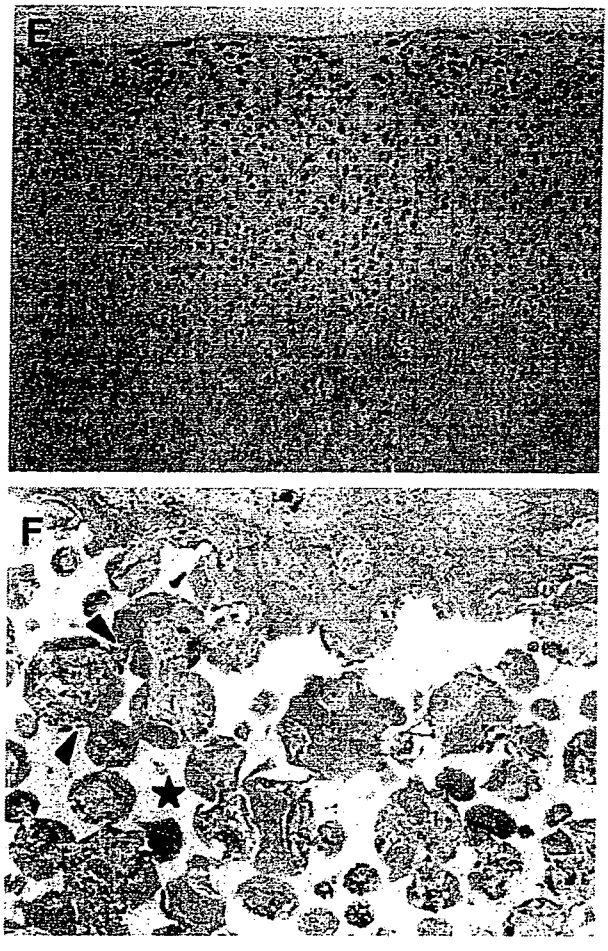

Fig. 5. (*continued*).

microscopically so well integrated with the surrounding host cartilage, the histological analysis revealed a slight discrepancy between safranin-O staining and immunoreactivity for type-II collagen [Fig. 6(J, L)]. This may be accounted for by the fact that chondrocytes near the junction with host cartilage produced less matrix than did those located more centrally within the regenerated tissue, where staining with safranin-O was absent only from the superficial zone, as in normal articular cartilage.

Cbfa1, a member of the Runt-domain family of transcriptional factors, is expressed not only in all osteoblasts, but also in chondrocytes and in earlier prechondrogenic mesenchymal condensations[47–49]. Furthermore, Cbfa1 is known to play an essential role in the differentiation not only of osteoblasts but also of chondrocytes, both at an early and a later stage of the process[50,51]. CD105 is a putative cell-surface marker for MSCs, which have the ability to undergo chondrogenesis, osteogenesis and adipogenesis[52,53]. One week after implantation, numerous cuboidal osteoblasts migrated into the pores of the IP-CHA scaffold from the host bone marrow (Fig. 3). And within peripheral pores, they had already begun to form bone tissue. The subchondral space above the IP-CHA scaffold was filled with an agglomeration of rounded fibroblast-like cells, which registered positive for Cbfa1 and/or CD105. They appeared to have migrated from the adjacent bone marrow, either directly, or indirectly via the interconnecting pores of the IP-CHA. These findings suggest that the aggregating fibroblast-like cells might have the potential for chondro/osteogenesis.

According to our findings, one of the keys to successful articular cartilage regeneration might be the activation of a subchondral repair process, thereby enabling chondroblastic/osteoblastic cells to effectively aggregate within the subchondral space. In rabbits, small, 3-mm-diameter, full-thickness articular cartilage defects heal spontaneously with repair tissue, which is composed of hyaline-like or fibrous cartilage. In adolescent rabbits (approximately 3 months old), osteochondral defects repair better and more rapidly than do those in adults[34,54]. Furthermore, adolescent rabbits have a larger population of metabolically active bone-marrow MSCs. Hence, in the present study, we established a large (4-mm-diameter) full-thickness defect model, it being necessary to exceed the upper limit (3 mm in diameter) for spontaneous repair. And since our system involved no cell-expansion step *in vitro*, the adolescent (rather than the adult) rabbit model was considered to be advantageous in its possession of a larger population of metabolically active bone-marrow MSCs.

A basic requirement for biomaterials is that they be non-carcinogenic and elicit no inflammatory reaction due to cytotoxicity or immunogenicity[55]. The BMP/PLA–PEG/IP-CHA composite is believed to meet these criteria. The PLA and PEG homopolymers and hydroxyapatite have been shown to be compatible and safe for clinical applications[30,56]. In addition to these safety features, it is crucial that biomaterials are easy to handle in clinical settings.

Table III
Results of the histological scoring

Group	No. of defects	Cell morphology	Matrix-staining	Structural integrity	Surface regularity	Thickness	Reconstruction of subchondral bone	Integration with adjacent cartilage	Total score
Group I: 3 weeks	6	3.6 ± 0.5*	2.0 ± 0	1.3 ± 0.5	2.0 ± 0.9	1.2 ± 0.4	0.8 ± 0.7	1.8 ± 0.4§	12.8 ± 2.4*
Group II: 3 weeks	6	1.7 ± 0.5	1.0 ± 0.6	0.5 ± 0.5	0.5 ± 0.5	0.7 ± 0.5	0.5 ± 0.4	1.0 ± 0.6§	5.8 ± 2.6
Group III: 3 weeks	6	2.2 ± 0.8	1.3 ± 0.5	0.5 ± 0.5	0.7 ± 0.4	1.0 ± 0	0.5 ± 0.4	1.2 ± 0.8§	7.2 ± 2.2
Group IV: 3 weeks	6	1.3 ± 0.5	0.8 ± 0.4	0.7 ± 0.5	1.3 ± 0.5	0.5 ± 0.3	0.5 ± 0.3	0.5 ± 0.3	5.1 ± 1.1
Group I: 6 weeks	6	3.8 ± 0.4*	2.3 ± 0.5*	1.5 ± 0.5§	2.2 ± 1.0	1.2 ± 0.4§	1.8 ± 0.4§	1.5 ± 0.5	15.0 ± 2.1*
Group II: 6 weeks	6	1.8 ± 0.4	1.5 ± 0.5	1.2 ± 0.4	1.5 ± 0.5	1.2 ± 0.4	1.3 ± 0.5§	1.2 ± 0.4	9.7 ± 1.2
Group III: 6 weeks	6	1.7 ± 1.0	1.0 ± 0.8	0.8 ± 0.4	1.7 ± 0.5	0.7 ± 0.5	1.3 ± 0.5§	1.2 ± 0.4	8.3 ± 3.0
Group IV: 6 weeks	6	1.5 ± 0.5	0.5 ± 0.4	0.5 ± 0.5	1.3 ± 0.5	0.7 ± 0.5	0.5 ± 0.3	0.8 ± 0.4	5.7 ± 1.9

Values represent the average score ± SD for each category. *$P < 0.01$ vs groups II, III, and IV. §$P < 0.01$ vs group IV.

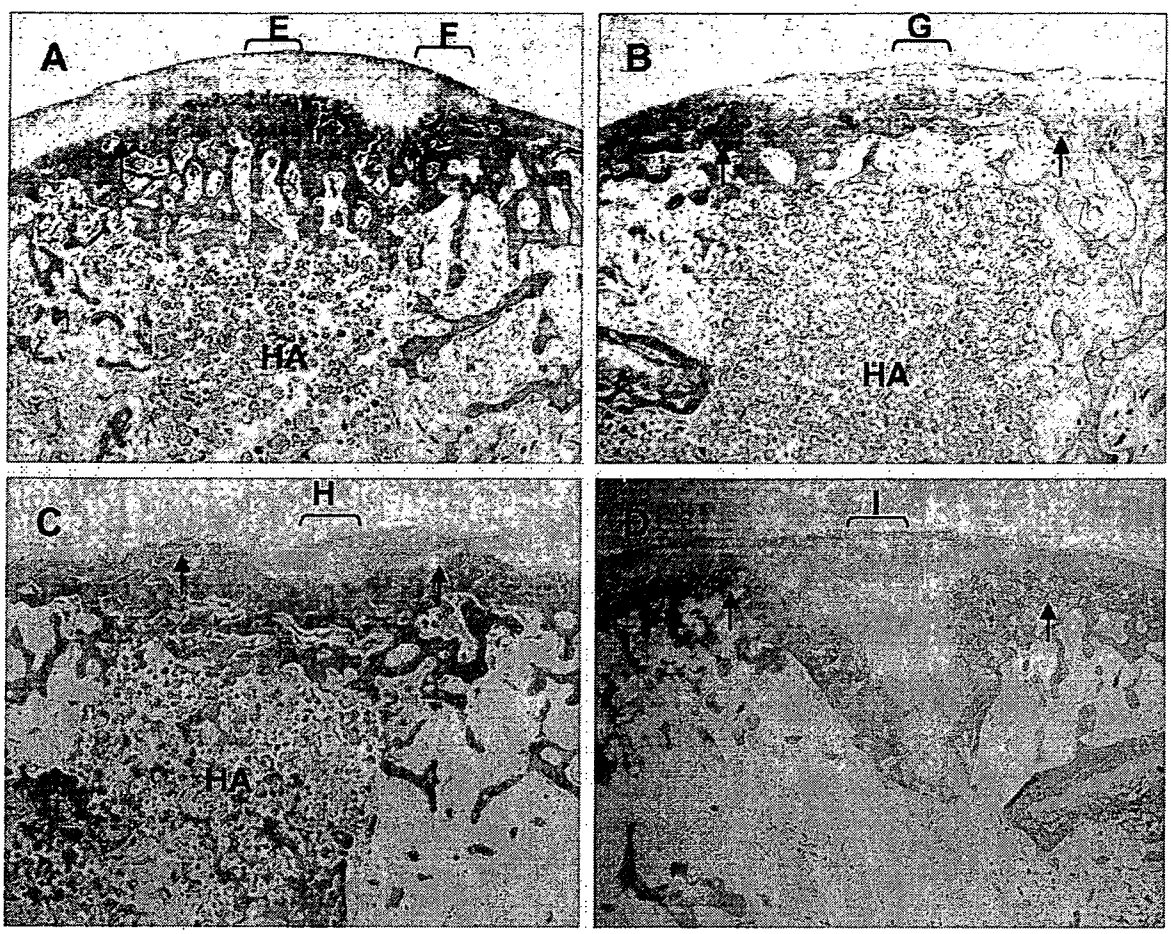

Fig. 6. Histological photomicrographs of defects 6 weeks after implantation with either the BMP/PLA–PEG/IP-CHA composite [(group I) A, E, F, J–L], the PLA–PEG/IP-CHA composite [(group II) B, G], or IP-CHA alone [(group III) C, H], and in the absence of treatment [empty (group IV) D, I]. Arrows indicate the margins of the defect. HA represents the implanted IP-CHA scaffold. Highly magnified images of the regions indicated in (A–D) are represented in (E–I). (A) The defect treated with the BMP/PLA–PEG/IP-CHA composite (group I) was filled with regenerated subchondral bone, which also penetrated the pores of the implant. The subchondral bone was covered with a layer of regenerated cartilage tissue of almost normal thickness. (B, C) In the control groups (group II and III), the defects were filled with a hypercellular type of fibrous tissue with regeneration of subchondral bone. The surface the repaired tissue was rough. (D) Without treatment (group IV), the defect site was predominantly replaced by thick fibrocartilage tissue with a thin layer of irregular subchondral bone. (E) The central region of the regenerated articular cartilage layer (group I). The repaired tissue has a hyaline-like appearance and is undergoing organization into vertical columns. The four horizontal strata characteristic of normal articular cartilage are apparent. (F) The junction between host and regenerated cartilage is continuous, and very little fibrillation of the articular surface is apparent (group I). (G–I) The repaired tissue is mainly of a fibrous nature (group II–IV). (J–L) Safranin-O staining (J), and immunostaining for type-I collagen (K) and type-II collagen (L) at the junction between host and the regenerated cartilage (group I). Magnification: (A–D) = 10×; (E–I) = 100×; (J–L) = 40×. (A–I): H&E staining.

Current techniques using cultured chondrocyte suspensions or collagen gels are complicated by problems associated with cell retention. Our composite material circumvents these problems. Furthermore, our material may be shaped into a "ready-to-use" form. It is possible to adjust its size and shape to suit the dimensions of the defect prior to implantation.

In conclusion, we have successfully induced the repair of articular cartilage defects within a relatively short period of time by combining rhBMP-2 with two biomaterials: IP-CHA as a scaffold and PLA–PEG as a carrier for rhBMP-2. The BMP/PLA–PEG/IP-CHA composite represents a new and promising technology for the engineering of articular cartilage. Clinical applications for the treatment of both osteoarthritis and articular cartilage injuries are also anticipated. Further studies involving long-term observations in both adolescent and adult animals are currently underway.

Acknowledgments

The authors thank Toshiba Ceramics Co., Ltd. for supplying the materials used in this study and for their technical assistance. We also thank Miss K. Asai for her technical assistance. This study was partially supported by grants from the Japanese Ministry of Health and Welfare, the Japanese Ministry of Education, Science and Culture, the Uehara Memorial Foundation, the New Energy and

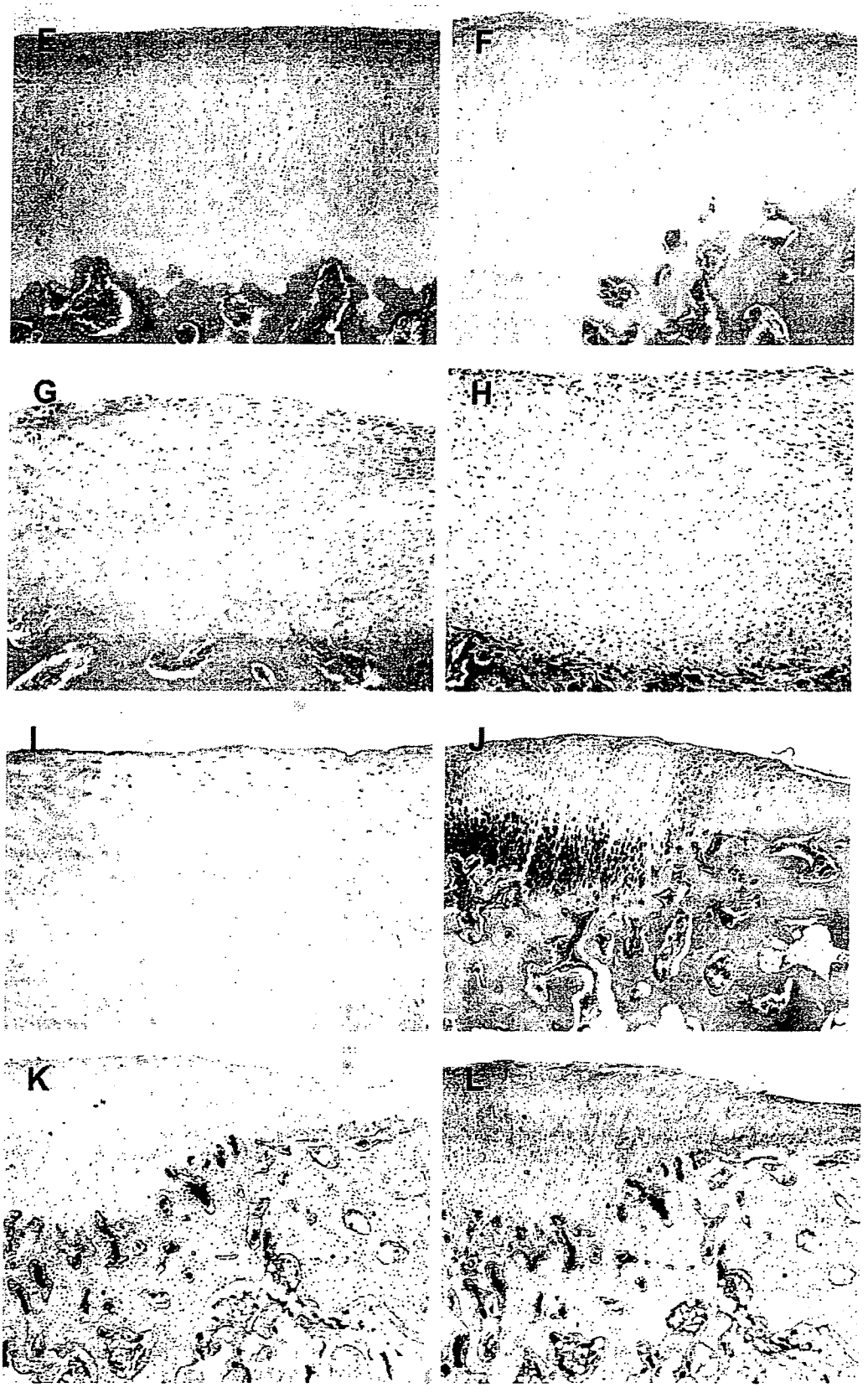

Fig. 6. (*continued*).

Industrial Technology Development Organization, the Japan Orthopaedics and Traumatology Foundation (No.0122), and JSPS Research Fellowships for Young Scientists (No. 04920).

References

1. Newman AP. Articular cartilage repair. Am J Sports Med 1998;26:309–24.
2. Lee CR, Grodzinsky AJ, Hsu HP, Spector M. Effects of a cultured autologous chondrocyte-seeded type II collagen scaffold on the healing of a chondral defect in a canine model. J Orthop Res 2003;21:272–81.
3. van Susante JL, Buma P, Homminga GN, van den Berg WB, Veth RP. Chondrocyte-seeded hydroxyapatite for repair of large articular cartilage defects. A pilot study in the goat. Biomaterials 1998;19:2367–74.
4. Mainil-Varlet P, Rieser F, Grogan S, Mueller W, Saager C, Jakob RP. Articular cartilage repair using a tissue-engineered cartilage-like implant: an animal study. Osteoarthritis Cartilage 2001;9:S6–S15.
5. Litzke LE, Wagner E, Baumgaertner W, Hetzel U, Josimovic-Alasevic O, Libera J. Repair of extensive articular cartilage defects in horses by autologous chondrocyte transplantation. Ann Biomed Eng 2004; 32:57–69.
6. Pittenger MF, Mackay AM, Beck SC, Jaiswal RK, Douglas R, Mosca JD, *et al.* Multilineage potential of adult human mesenchymal stem cells. Science 1999; 284:143–7.
7. Kadiyala S, Young RG, Thiede MA, Bruder SP. Culture expanded canine mesenchymal stem cells possess osteochondrogenic potential *in vivo* and *in vitro*. Cell Transplant 1997;6:125–34.
8. Wakitani S, Goto T, Pineda SJ, Young RG, Mansour JM, Caplan AI, *et al.* Mesenchymal cell- based repair of large, full-thickness defects of articular cartilage. J Bone Joint Surg Am 1994;76-A:579–92.
9. Butnariu-Ephrat M, Robinson D, Mendes DG, Halperin N, Nevo Z. Resurfacing of goat articular cartilage by chondrocytes derived from bone marrow. Clin Orthop 1998;330:234–43.
10. Steadman JR, Rodkey WG, Rodrigo JJ. Microfracture: surgical technique and rehabilitation to treat chondral defects. Clin Orthop 2001;391S:362–9.
11. Kumai T, Takakura Y, Higashiyama I, Tamai S. Arthroscopic drilling for the treatment of osteochondral lesions of the tarus. J Bone Joint Surg Am 1999;81-A: 1229–35.
12. Shea CM, Edgar CM, Einhorn TA, Gerstenfeld LC. BMP treatment of C3H10T1/2 mesenchymal stem cells induces both chondrogenesis and osteogenesis. J Cell Biochem 2003;90:1112–27.
13. Carlberg AL, Pucci B, Rallapalli R, Tuan RS, Hall DJ. Efficient chondrogenic differentiation of mesenchymal cells in micromass culture by retroviral gene transfer of BMP-2. Differentiation 2001;67:128–38.
14. Zuscik MJ, Baden JF, Wu Q, Sheu TJ, Schwarz EM, Drissi H, *et al.* 5-azacytidine alters TGF-beta and BMP signaling and induces maturation in articular chondrocytes. J Cell Biochem 2004;92:316–31.
15. Mason JM, Breitbart AS, Barcia M, Porti D, Pergolizzi RG, Grande DA. Cartilage and bone regeneration using gene-enhanced tissue engineering. Clin Orthop 2000; 379S:S171–8.
16. Issack PS, DiCesare PE. Recent advances toward the clinical application of bone morphogenetic proteins in bone and cartilage repair. Am J Orthop 2003;32: 429–36.
17. King GN. The importance of drug delivery to optimize the effect of bone morphogenetic proteins during periodontal regeneration. Curr Pharm Biotechnol 2001;2:131–42.
18. Fiedler J, Roderer G, Gunther KP, Brenner RE. BMP-2, BMP-4, and PDGF-bb stimulate chemotactic migration of primary human mesenchymal progenitor cells. J Cell Biochem 2002;87:305–12.
19. Postlethwaite AE, Raghow R, Stricklin G, Ballou L, Sampath TK. Osteogenic protein-1, a bone morphogenic protein member of the TGF-beta superfamily, shares chemotactic but not fibrogenic properties with TGF-beta. J Cell Physiol 1994;161:562–70.
20. Muckle DS, Minns RJ. Biological response to woven carbon fibre pads in the knee: a clinical and experimental study. J Bone Joint Surg Br 1989;71:60–2.
21. Buma P, Pieper JS, van Tienen T, van Susante JL, van der Kraan PM, Veerkamp JH, *et al.* Cross-linked type I and type II collagenous matrices for the repair of full-thickness articular cartilage defects-a study in rabbits. Biomaterials 2003;24:3255–63.
22. Cohen SB, Meirisch CM, Wilson HA, Diduch DR. The use of absorbable co-polymer pads with alginate and cells for articular cartilage repair in rabbits. Biomaterials 2003;24:2653–60.
23. Ushida T, Furukawa K, Toita K, Tateishi T. Three-dimensional seeding of chondrocytes encapsulated in collagen gel into PLLA scaffolds. Cell Transplant 2002;11:489–94.
24. Chiroff RT, White RA, White EW, Weber JN, Roy D. The restoration of the articular surfaces overlying Replamineform porous biomaterials. J Biomed Mater Res 1977;11:165–78.
25. Suominen E, Aho AJ, Vedel E, Kangasniemi I, Uusipaikka E, Yli-Urpo A. Subchondral bone and cartilage repair with bioactive glasses, hydroxyapatite, and hydroxyapatite-glass composite. J Biomed Mater Res 1996;32:543–51.
26. Miyamoto S, Takaoka K, Okada T, Yoshikawa H, Hashimoto J, Suzuki S, *et al.* Evaluation of polylactic acid homopolymers as carriers for bone morphogenetic protein. Clin Orthop 1992;278:274–85.
27. Saito N, Okada T, Horiuchi H, Murakami N, Takahashi J, Nawata M, *et al.* Biodegradable poly-D,L-lactic acid–polyethylene glycol blocks copolymers as a BMP delivery system for inducing bone. J Bone Joint Surg Am 2001;81-A:92–8.
28. Saito N, Okada T, Horiuchi H, Murakami N, Takahashi J, Nawata M, *et al.* A biodegradable polymer as a cytokine delivery system for including bone formation. Nat Biotechnol 2001;19:332–5.
29. Saito N, Okada T, Toba S, Miyamoto S, Takaoka K. New synthetic absorbable polymers as BMP carriers: plastic properties of poly-D,L-lactic acid–polyethylene glycol block copolymers. J Biomed Mater Res 1999; 47:104–10.
30. Tamai N, Myoui A, Tomita T, Nakase T, Tanaka J, Ochi T, *et al.* Novel hydroxyapatite ceramics with an interconnective porous structure exhibit superior osteoinduction *in vivo*. J Biomed Mater Res 2002; 59:110–7.
31. Nishikawa M, Myoui A, Ohgushi H, Ikeuchi M, Tamai N, Yoshikawa H. Bone tissue engineering using novel

interconnected porous hydroxyapatite ceramics combined with marrow mesenchymal cells: quantitative and three-dimensional image analysis. Cell Transplant 2004;13:367–76.
32. Kaito T, Myoui A, Takaoka K, Saito N, Nishikawa M, Tamai N, *et al.* Potentiation of the activity of bone morphogenetic protein-2 in bone regeneration by a PLA–PEG/hydroxyapatite composite. Biomaterials 2005;26:73–9.
33. Akita S, Tamai N, Myoui A, Nishikawa M, Kaito T, Takaoka K, *et al.* Capillary vessel network integration by inserting a vascular pedicle enhances bone formation in tissue-engineered bone using interconnected porous hydroxyapatite ceramics. Tissue Eng 2004;10:789–95.
34. Wei X, Gao J, Messner K. Maturation-dependent repair of untreated osteochondral defects in the rabbit knee joint. J Biomed Mater Res 1997;34:63–72.
35. Kumagai K, Saito T, Koshino T. Articular cartilage repair of rabbit chondral defect: promoted by creation of periarticular bony defect. J Orthop Sci 2003;8: 700–6.
36. Schaefer D, Martin I, Jundt G, Seidel J, Heberer M, Grodzinsky A, *et al.* Tissue-engineered composites for the repair of large osteochondral defects. Arthritis Rheum 2002;46:2524–34.
37. Ikeuchi M, Dohi Y, Horiuchi K, Ohgushi H, Noshi T, Yoshikawa T, *et al.* Recombinant human bone morphogenetic protein-2 promotes osteogenesis within atelopeptide type I collagen solution by combination with rat cultured marrow cells. J Biomed Mater Res 2002;60:61–9.
38. Hegyi L, Gannon FH, Glaser DL, Shore EM, Kaplan FS, Shanahan CM. Stromal cells of fibrodysplasia ossificans progressiva lesions express smooth muscle lineage markers and the osteogenic transcription factor Runx2/Cbfa-1: clues to a vascular origin of heterotopic ossification? J Pathol 2003;201:141–8.
39. Wakitani S, Imoto K, Yamamoto T, Saito M, Murata N, Yoneda M. Human autologous culture expanded bone marrow mesenchymal cell transplantation for repair of cartilage defects in osteoarthritic knees. Osteoarthritis Cartilage 2002;10:199–206.
40. Cook SD, Patron LP, Salkeld SL, Rueger DC. Repair of articular cartilage defects with osteogenic protein-1 (BMP-7) in dogs. J Bone Joint Surg Am 2003;85-A: 116–23.
41. Sellers RS, Peluso D, Morris EA. The effect of recombinant human bone morphogenetic protein-2 (rhBMP-2) on the healing of full-thickness defects of articular cartilage. J Bone Joint Surg Am 1997;79: 1452–63.
42. Hidaka C, Goodrich LR, Chen CT, Warren RF, Crystal RG, Nixon AJ. Acceleration of cartilage repair by genetically modified chondrocytes over expressing bone morphogenetic protein-7. J Orthop Res 2003;21: 573–83.
43. Sellers RS, Zhang R, Glasson SS, Kim HD, Peluso D, D'Augusta DA, *et al.* Repair of articular cartilage defects one year after treatment with recombinant human bone morphogenetic protein-2 (rhBMP-2). J Bone Joint Surg Am 2000;82:151–61.
44. Hunziker EB, Driesang IM, Morris EA. Chondrogenesis in cartilage repair is induced by members of the transforming growth factor-beta superfamily. Clin Orthop 2001;391S:171–81.
45. Frenkel SR, Saadeh PB, Mehrara BJ, Chin GS, Steinbrech DS, Brent B, *et al.* Transforming growth factor beta superfamily members: role in cartilage modeling. Plast Reconstr Surg 2000;105:980–90.
46. Kim HD, Valentini RF. Retention and activity of BMP-2 in hyaluronic acid-based scaffolds *in vitro*. J Biomed Mater Res 2002;59:573–84.
47. Inada M, Yasui T, Nomura S, Miyake S, Deguchi K, Himeno M, *et al.* Maturational disturbance of chondrocytes in Cbfa1-deficient mice. Dev Dyn 1999;214: 279–90.
48. Otto F, Thornell AP, Crompton T, Denzel A, Gilmour KC, Rosewell IR, *et al.* Cbfa1, a candidate gene for cleidocranial dysplasia syndrome, is essential for osteoblastic differentiation and bone development. Cell 1997;89:765–71.
49. de Crombrugghe B, Lefebvre V, Nakashima K. Regulatory mechanisms in the pathways of cartilage and bone formation. Curr Opin Cell Biol 2001;13:721–7.
50. Stricker S, Fundele R, Vortkamp A, Mundlos S. Role of Runx genes in chondrocyte differentiation. Dev Biol 2002;245:95–108.
51. Kim IS, Otto F, Zabel B, Mundlos S. Regulation of chondrocyte differentiation by Cbfa1. Mech Dev 1999; 80:159–70.
52. Lodie TA, Blickarz CE, Devarakonda TJ, He C, Dash AB, Clarke J, *et al.* Systematic analysis of reportedly distinct populations of multipotent bone marrow-derived stem cells reveals a lack of distinction. Tissue Eng 2002;8: 739–51.
53. De Ugarte DA, Alfonso Z, Zuk PA, Elbarbary A, Zhu M, Ashjian P, *et al.* Differential expression of stem cell mobilization-associated molecules on multi-lineage cells from adipose tissue and bone marrow. Immunol Lett 2003;89:267–70.
54. Shapiro F, Koide S, Glimcher MJ. Cell origin and differentiation in the repair of full-thickness defects of articular cartilage. J Bone Joint Surg Am 1993;75: 532–53.
55. Langer R. Drug delivery and targeting. Nature 1998; 392:5–10.
56. Jeong B, Bae YH, Lee DS, Kim SW. Biodegradable block copolymers as injectable drug-delivery systems. Nature 1997;388:860–2.

ARTHRITIS & RHEUMATISM
Vol. 52, No. 12, December 2005, pp 3819–3828
DOI 10.1002/art.21425

Nurse-like Cells From Patients With Rheumatoid Arthritis Support the Survival of Osteoclast Precursors Via Macrophage Colony-Stimulating Factor Production

Hideki Tsuboi,[1] Nobuyuki Udagawa,[2] Jun Hashimoto,[1] Hideki Yoshikawa,[1] Naoyuki Takahashi,[2] and Takahiro Ochi[3]

Objective. **To elucidate the role of nurse-like cells (NLCs) obtained from rheumatoid arthritis (RA) patients in bone loss during progressive synovial expansion.**

Methods. **CD14+ monocytes were cocultured with NLCs for 4 weeks and collected as NLC-supported CD14+ (NCD14+) monocytes. To determine their ability to differentiate into osteoclasts, NCD14+ monocytes were further cultured with macrophage colony-stimulating factor (M-CSF) together with RANKL or tumor necrosis factor α (TNFα). NCD14+ monocytes were also cocultured with SaOS-4/3 cells, which were shown to support osteoclastogenesis in response to parathyroid hormone (PTH). CD14+ monocytes were cocultured with SaOS-4/3 cells to elucidate how SaOS-4/3 cells and NLCs supported CD14+ monocytes for a long period. Synovial expansion adjacent to bone in RA patients was examined immunohistochemically to detect osteoclast precursors such as NCD14+ monocytes.**

Results. **NLCs supported the survival of CD14+ monocytes for 4 weeks. NCD14+ as well as CD14+ monocytes differentiated into osteoclasts in the presence of M-CSF together with RANKL or TNFα. NCD14+ monocytes also differentiated into osteoclasts in PTH-treated cocultures with SaOS-4/3 cells. SaOS-4/3 cells supported the survival of CD14+ monocytes for 4 weeks in the presence, but not absence, of PTH. Treatment of SaOS-4/3 cells with PTH up-regulated the expression of M-CSF messenger RNA. Neutralizing antibodies against M-CSF inhibited the NLC-supported survival of CD14+ monocytes. CD68+ monocytes and M-CSF+ fibroblast-like synoviocytes were colocalized in regions adjacent to the destroyed bone of RA patients.**

Conclusion. **Our findings suggest that NLCs are involved in RA-induced bone destruction by maintaining osteoclast precursors via production of M-CSF.**

Osteoclasts, the multinucleated cells that resorb bone, originate from the monocyte/macrophage lineage. Recent studies have established that bone-forming osteoblasts (or, bone marrow–derived stromal cells) are involved in the differentiation and function of osteoclasts (1–4). Macrophage colony-stimulating factor (M-CSF), which is produced by osteoblasts, is an essential cytokine for osteoclast formation. Osteoblasts also express RANKL, another cytokine involved in osteoclast differentiation, as a membrane-associated cytokine. Osteoclast precursors express RANK (the receptor for RANKL), recognize RANKL expressed by osteoblasts through cell–cell interaction, and differentiate into osteoclasts in the presence of M-CSF (1–4). Osteoprotegerin (OPG), which is produced mainly by osteoblasts, is a soluble decoy receptor for RANKL and blocks osteoclastogenesis by inhibiting RANKL–RANK interactions (5,6). Bone resorption–stimulating hormones and cytokines enhance the expression of RANKL in osteoblasts. Recent studies have shown that tumor necrosis factor α (TNFα) stimulates osteoclast differentiation in the presence of M-CSF through a mechanism independent of the RANKL/RANK system (7) and that

Supported in part by a grant-in-aid from the Health Science Research grant from the Ministry of Health and Welfare of Japan.

[1]Hideki Tsuboi, MD, PhD, Jun Hashimoto, MD, PhD, Hideki Yoshikawa, MD, PhD: Osaka University Graduate School of Medicine, Suita, Japan; [2]Nobuyuki Udagawa, DDS, PhD, Naoyuki Takahashi, PhD: Matsumoto Dental University, Shiojiri, Japan; [3]Takahiro Ochi, MD, PhD: Osaka University Graduate School of Medicine, Suita, and National Hospital Organization, Sagamihara National Hospital, Sagamihara, Japan.

Address correspondence and reprint requests to Takahiro Ochi, MD, PhD, National Hospital Organization Sagamihara National Hospital, 18-1 Sakuradai, Sagamihara, Kanagawa 228-8522, Japan. E-mail: t-ochi@sagamihara-hosp.gr.jp.

Submitted for publication December 1, 2004; accepted in revised form August 18, 2005.

interleukin-1 (IL-1) acts directly on osteoclasts to induce bone-resorbing activity (8).

Rheumatoid arthritis (RA) is a chronic inflammatory disease characterized by arthritis affecting multiple joints and the progressive destruction of cartilage and bone (9). Osteoclasts activated by inflammatory cytokines are involved in bone destruction in RA. Recent studies have suggested that a progressive synovial expansion called pannus at sites of bone destruction plays important roles in osteoclastic bone resorption (10–12). In addition, osteoclasts formed from circulating precursors obtained from patients with RA have an increased bone-resorbing activity compared with those obtained from normal control subjects (13). However, the etiology of RA and the mechanism of bone destruction induced by RA have not yet been elucidated completely.

Nurse cells were first recognized in cell suspensions of dissociated thymus (14). Thymic nurse cells supported the differentiation and maturation of T cells. When bone marrow–derived T cell precursors were cocultured with thymic nurse cells, the T cell precursors crawled beneath the thymic nurse cell layers and differentiated into mature thymocytes. This phenomenon, known as pseudoemperipolesis, is peculiar to nurse cells and has been used to identify nurse-like cells (NLCs) in various tissues (15–17). We have established NLC lines from the synovium and bone marrow of patients with RA (16,17). NLCs showed characteristics similar to those of fibroblast-like synoviocytes. NLCs promoted the activation and differentiation of both B and T lymphocytes in coculture. It was also shown that stromal cell–derived factor 1 and CD106 (vascular cell adhesion molecule 1) were involved in the formation and maintenance of B cell pseudoemperipolesis by RA fibroblast-like synoviocytes (18).

We recently showed that NLCs promoted the survival of peripheral blood monocytes as well as B cells (19). Monocytes supported by NLCs possessed tartrate-resistant acid phosphatase (TRAP; a marker enzyme of osteoclasts) activity and differentiated into osteoclast-like multinucleated cells in response to some cytokines, including RANKL. However, it is not clear how fibroblast-like synoviocytes are involved in bone destruction in RA. In the present study, we examined the ability of monocytes supported for 4 weeks by NLCs to differentiate into osteoclasts in comparison with the ability of freshly isolated peripheral blood monocytes to do so. We also examined how NLCs support the survival of osteoclast precursors for a long period of culture.

MATERIALS AND METHODS

Chemicals. Recombinant human M-CSF (Leukoprol) was obtained from Kyowa Hakko Kogyo (Tokyo, Japan), recombinant soluble RANKL and OPG from PeproTech (London, UK), and recombinant human TNFα and neutralizing antibody against human M-CSF from Genzyme (Minneapolis, MN). We purchased 1α,25-dihydroxyvitamin D_3 (1α,25$[OH]_2D_3$) and prostaglandin E_2 (PGE_2) from Wako (Osaka, Japan). Human parathyroid hormone 1–34 (PTH 1–34) was obtained from Peptide Institute (Osaka, Japan). A monoclonal antibody against vitronectin receptors (VNRs; human CD51/61 complex) (23C6) was purchased from Serotec (Oxford, UK). A monoclonal antibody against human CD68 (KP1) and polyclonal antibodies against human M-CSF were from Dako (Glostrup, Denmark) and Santa Cruz Biotechnology (Santa Cruz, CA), respectively.

Cells and the coculture system. CD14+ monocytes were isolated from peripheral blood using anti-CD14 antibody–coated beads, as described previously (19). NLCs were established from synovium and bone marrow obtained from patients with RA. NLCs were cultured in Dulbecco's modified Eagle's medium (DMEM; Gibco BRL, Gaithersburg, MD) supplemented with 10% fetal calf serum (FCS; Hyclone, Logan, UT). Half of the medium was replaced weekly with the fresh medium. SaOS-4/3 cells were established from the SaOS-2 human osteosarcoma cell line by transfection with human PTH/PTH-related protein receptor complementary DNA (cDNA) (20). SaOS-4/3 cells support human osteoclast formation in response to PTH in cocultures with human peripheral blood mononuclear cells (20,21).

CD14+ monocytes (5×10^5 cells/well) were cocultured with NLCs (4×10^4 cells/well) or with SaOS-4/3 cells (4×10^4 cells/well) in the presence or absence of PTH ($10^{-8}M$) for 4 weeks in DMEM supplemented with 10% FCS in 12-well plates. Neutralizing antibodies against human M-CSF (final concentrations 50 ng/ml, 500 ng/ml, and 5,000 ng/ml) were added to some cocultures with NLCs. The culture medium was replaced every 3 days with the fresh medium. The number of CD14+ monocytes recovered from the coculture with NLCs or SaOS-4/3 cells was counted every week. After coculture for 4 weeks, the floating or weakly adherent CD14+ monocytes were harvested as NLC-supported CD14+ cells, or NCD14+ monocytes, by gently washing the culture with DMEM supplemented with 10% FCS. The ability of NCD14+ monocytes and CD14+ monocytes to differentiate into osteoclasts was compared as described below.

Osteoclast formation assay. NCD14+ monocytes (1×10^4/well) and freshly isolated CD14+ monocytes (3×10^4/well) were cultured in the presence or absence of M-CSF (25 ng/ml), RANKL (40 ng/ml), TNFα (20 ng/ml), or OPG (100 ng/ml) in α-minimum essential medium (α-MEM; Gibco) supplemented with 10% FCS in a 96-well plate. NCD14+ monocytes (2×10^4/well) were also cocultured with SaOS-4/3 cells (1×10^4/well) in 48-well plates in α-MEM supplemented with 10% FCS in the presence or absence of PTH ($10^{-8}M$). Some cultures were treated with OPG (100 ng/ml). After a specific period of time, cells were fixed and stained for TRAP using a TRAP staining kit obtained from Hokudo (Hokkaido, Japan).

For immunohistochemical staining, cells were fixed with cold methanol:acetone (50:50 volume/volume) for 10

Table 1. Sequences of polymerase chain reaction primers*

	Primers (5′–3′)		
	Sense	Antisense	Expected product size, bp
CD14	TCCCCACAAGTTCCCGGCCATC	TCCACCTCGGGCAGCTCGTCAG	315
CD68	TTCCCCCACGCAGCAAAGTGGA	ACCCCAAACCCCCTCAGTGCCC	362
CTR	TCCATGGACCTGTCATGGCGGC	TTGGCGCTTCACGGTGGTTTGG	314
M-CSF	GCTTTGCTGAATGCTCCAGC	CAGAGGGACATTGGACAAACG	308, 1,201
OPG	CCGCCTCCAAGCCCCTGAGGTT	ACACGCGGTTGTGGGTGCGATT	400
RANK	CTTCGCGTCTGTGGCCCTGGTG	CCTGGCATCTTCGCCTTGTGCG	319
RANKL	GCATGGCCCCAACGGTACACGA	TCAGCTGCGAAGGGGCACATGA	237
TNFRI	TTCTTGCCCCCACCCGTCCATC	CCAGCCATCCAGGGCCACCTTC	359
GAPDH	TGCTCTTGCTGGGGCTGGTGGT	TGCCAAGGCTGTGGGCAAGGTC	400

* CTR = calcitonin receptor; M-CSF = macrophage colony-stimulating factor; OPG = osteoprotegerin; TNFRI = tumor necrosis factor receptor I.

minutes and incubated with a monoclonal antibody against VNR, an osteoclast-associated antigen. The bound antibodies were visualized with biotinylated secondary antibodies, avidin–biotin–conjugated peroxidase, and an aminoethylcarbazole substrate kit (Histofine; Nichirei, Tokyo, Japan).

For the pit-formation assay, NCD14+ and CD14+ monocytes were cultured on dentin slices in α-MEM supplemented with 10% FCS in 48-well plates (1 slice/well) in the presence or absence of several of the factors described above. After 21 days, dentin slices were stained with Mayer's hematoxylin solution to detect resorption pits.

Reverse transcription–polymerase chain reaction (RT-PCR) analysis. Total RNA was extracted from CD14+ (5×10^6 cells) and NCD14+ (5×10^5 cells) monocytes using an RNeasy Mini kit (Qiagen, Hilden, Germany) according to the manufacturer's directions. After treatment with DNase I (Life Technologies, Rockville, MD), single-stranded cDNA was synthesized using 2 μg of each RNA sample, 100 ng of random primers, and 4 units of Omniscript reverse transcriptase (Qiagen) in a total reaction volume of 20 μl. Amplification was performed with 0.5 units of Ex *Taq* (Takara, Shiga, Japan) in a total reaction volume of 20 μl containing 1× reaction buffer, 200 μM of each dNTP, and 10 pmoles of each primer. The PCR conditions were as follows: initial denaturation for 2 minutes at 94°C, then 30 cycles of 30 seconds each at 94°C and 72°C (annealing at 72°C).

To determine the expression of calcitonin receptor (CTR) messenger RNA (mRNA), NCD14+ monocytes (4×10^5/well) were cocultured with SaOS-4/3 cells (2×10^5/well) in 6-well plates with or without PTH ($10^{-8}M$) and with or without PTH ($10^{-8}M$) plus OPG (100 ng/ml). Total RNA extracted from the coculture was subjected to RT-PCR analysis of CTR mRNA expression.

To determine the expression of RANKL, OPG, and M-CSF mRNA, NLCs (5×10^6/dish) or SaOS-4/3 cells (5×10^6/dish) were cultured for 3 days in a 10-cm culture dish in the presence or absence of PTH ($10^{-8}M$), PGE_2 ($10^{-6}M$), or $1\alpha,25(OH)_2D_3$ ($10^{-8}M$). Total RNA was then extracted from the cells and subjected to a RT-PCR analysis of RANKL, OPG, and M-CSF mRNA expression.

A fragment of GAPDH cDNA was amplified as a control in all reactions. Aliquots of the PCR products were subjected to electrophoresis on 1.5% agarose gels and visualized by staining with ethidium bromide. In all cases, reproducibility was confirmed in triplicate experiments. The primer sets for CD14, CD68, CTR, M-CSF, OPG, RANK, RANKL, TNF receptor I (TNFRI), and GAPDH are shown in Table 1.

Immunohistochemical and TRAP staining of tissue samples from RA patients. Tissue samples, including the bone–synovium interface, were obtained during total knee arthroplasty in 5 RA patients, after they provided informed consent. The American College of Rheumatology (formerly, the American Rheumatism Association) criteria were used for the diagnosis of RA (22). The clinical features of the RA patients are summarized in Table 2.

Tissue samples were fixed in 4% paraformaldehyde at 4°C for 24 hours and decalcified in 20% EDTA for 2 hours in a microwave oven (H2800 Microwave Processor; Energy Beam Sciences, Agawam, MA) at 50°C and then for 22 hours at 4°C (23). Next, the samples were dehydrated through an ethanol series and embedded in paraffin. Sections (4 μm thick) were cut with a microtome and stained with TRAP and immunohistochemical stains. Immunohistochemical staining was performed by the streptavidin–biotin–peroxidase complex technique using a Histofine SAB-PO kit (Nichirei) according to the manufacturer's instructions. Briefly, after blocking endogenous peroxidase and nonspecific antigens, tissue sections were incu-

Table 2. Characteristics of the rheumatoid arthritis patients at the time of surgery*

No. of men/women	0/5
Age, mean (range) years	62.2 (57–68)
CRP, mean (range) mg/dl	1.76 (0.9–4.4)
Disease duration, mean (range) years	20.8 (14–28)
No. taking NSAIDs	5
Treatment during previous 6 months, no. of patients	
Gold salts	0
Bucillamine	0
Methotrexate	4
Prednisolone	3

* CRP = C-reactive protein; NSAIDs = nonsteroidal antiinflammatory drugs.

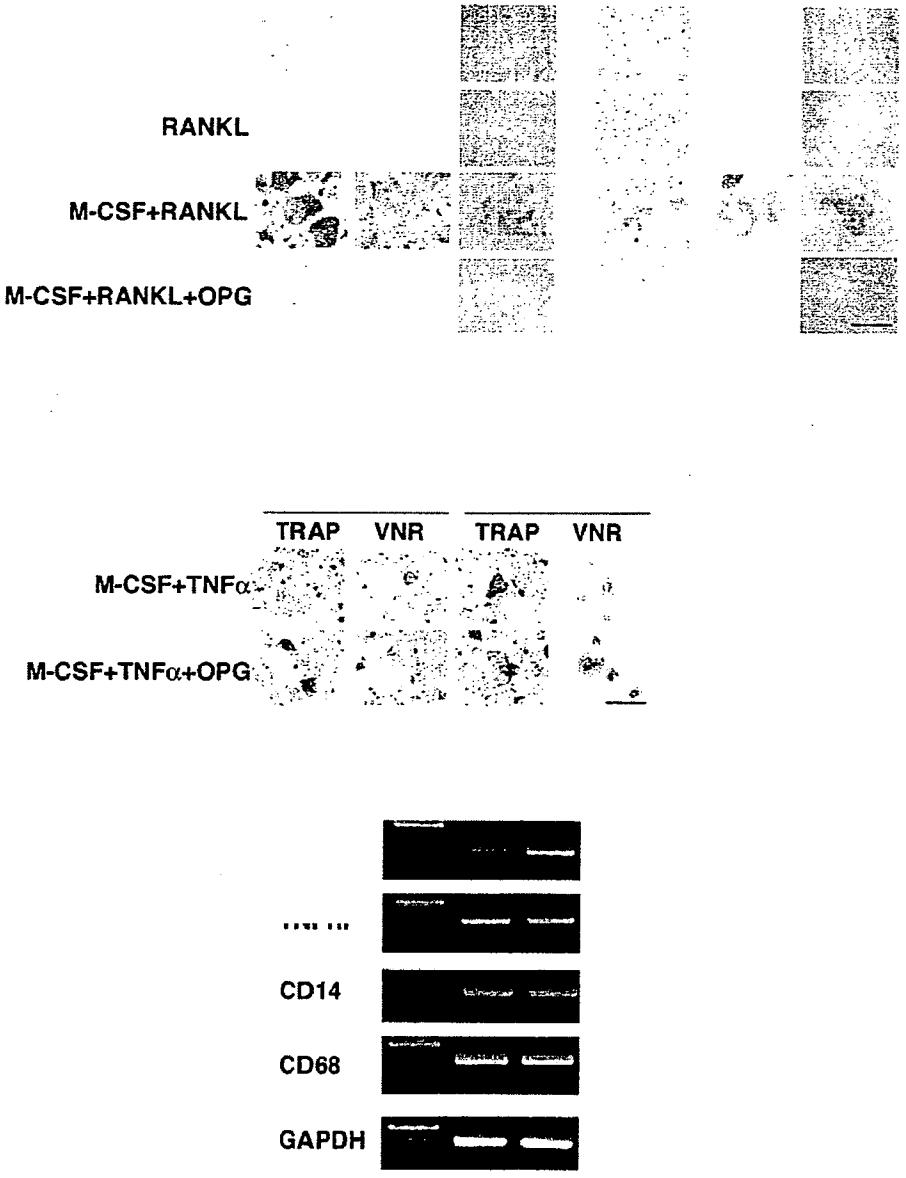

Figure 1. Osteoclast formation from CD14+ monocytes and nurse-like cell–supported CD14+ (NCD14+) monocytes. **A**, CD14+ monocytes were cultured for 7 days with or without macrophage colony-stimulating factor (M-CSF; 25 ng/ml), RANKL (40 ng/ml), M-CSF (25 ng/ml) plus RANKL (40 ng/ml), or M-CSF (25 ng/ml) plus RANKL (40 ng/ml) plus osteoprotegerin (OPG; 100 ng/ml). NCD14+ monocytes were similarly cultured for 14 days. Cultures were then fixed and stained for tartrate-resistant acid phosphatase (TRAP) or for vitronectin receptor (VNR). For the pit-formation assay, NCD14+ and CD14+ monocytes were cultured on dentin slices in the presence or absence of several of the factors described above. After 21 days in culture, dentin slices were stained with Mayer's hematoxylin to detect resorption pits. Bar = 100 μm. **B**, CD14+ and NCD14+ monocytes were cultured for 7 and 14 days, respectively, with M-CSF (25 ng/ml) plus tumor necrosis factor α (TNFα; 20 ng/ml) in the presence or absence of OPG (100 ng/ml). Cultures were stained for TRAP or VNR. Bar = 100 μm. **C**, Total RNA was extracted from CD14+ and NCD14+ monocytes, and the expression of mRNA for RANK, TNF receptor I (TNFRI), CD14, CD68, and GAPDH was analyzed by reverse transcription–polymerase chain reaction.

bated with primary antibodies against M-CSF and CD68 for 24 hours at 4°C. The sections were washed with phosphate buffered saline and incubated with the secondary antibody, followed by peroxidase-conjugated streptavidin (Nichirei). After a wash with phosphate buffered saline, the sections were incubated with 3,3′-diaminobenzidine tetrahydrochloride (Dojindo, Kumamoto, Japan) to detect peroxidase activity and then counterstained with hematoxylin. TRAP was detected using a TRAP staining kit (Hokudo).

Statistical analysis. The statistical significance of differences was analyzed using Student's *t*-test. *P* values less than 0.05 were considered significant. All results are representative of at least 3 individual experiments.

RESULTS

Cytokine-induced osteoclast formation from CD14+ and NCD14+ monocytes. CD14+ monocytes were prepared from peripheral blood, and NCD14+ monocytes were prepared from CD14+ monocytes and NLCs that had been cocultured for 4 weeks. CD14+ monocytes were cultured for 7 days with or without M-CSF, RANKL, M-CSF plus RANKL, or M-CSF plus RANKL plus OPG. Multinucleated cells positive for both TRAP and VNR were formed in the presence of M-CSF plus RANKL (Figure 1A). When CD14+ monocytes were cultured on dentin slices, resorption pits on the slices were observed only in the culture treated with M-CSF plus RANKL. Addition of OPG, a decoy receptor for RANKL, to the CD14+ culture treated with M-CSF plus RANKL inhibited the formation of TRAP+ and VNR+ multinucleated cells. Pit formation on dentin slices induced by M-CSF plus RANKL was inhibited by the addition of OPG to the CD14+ culture.

Similarly, NCD14+ monocytes differentiated into TRAP+ and VNR+ multinucleated cells in response to M-CSF plus RANKL (Figure 1A). The formation of TRAP+ and VNR+ multinucleated cells from NCD14+ monocytes was completely inhibited by the addition of OPG. However, a longer culture period was required to induce the multinucleated cells in NCD14+ cultures (7–14 days) than to induce them in CD14+ cultures (7 days). Resorption pits were also detected on dentin slices on which NCD14+ monocytes had been cultured in the presence of M-CSF plus RANKL.

Both CD14+ and NCD14+ monocytes differentiated into TRAP+ and VNR+ multinucleated cells in response to TNFα instead of RANKL in the presence of M-CSF (Figure 1B). OPG failed to inhibit the formation of TNFα-induced TRAP+ and VNR+ multinucleated cells in CD14+ and NCD14+ cultures. RT-PCR analysis showed that CD14+ and NCD14+ monocytes expressed similar levels of mRNA for the monocyte/macrophage-associated antigens CD14 and CD68 (Figure 1C). Both cell populations expressed mRNA for RANK (the receptor for RANKL) and TNFRI (the type I TNF receptor).

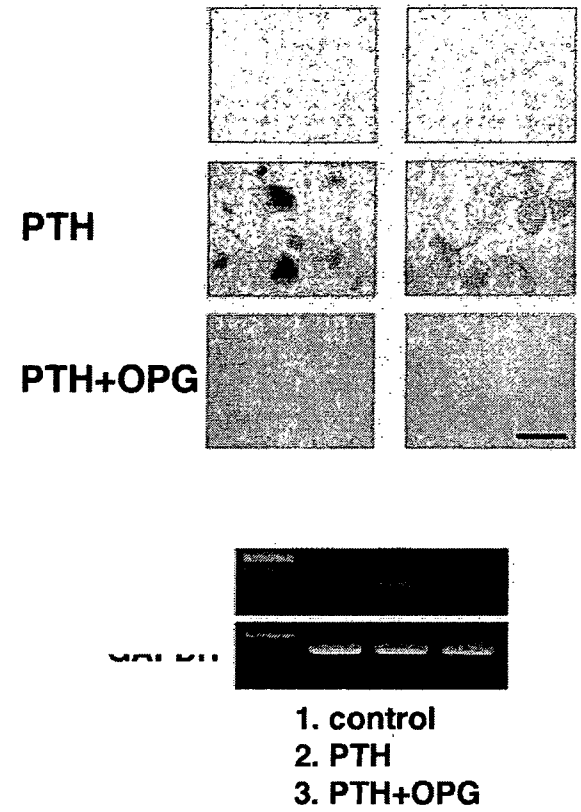

Figure 2. Osteoclast formation from nurse-like cell–supported CD14+ (NCD14+) monocytes in coculture with SaOS-4/3 cells. **A,** NCD14+ monocytes were cocultured with SaOS-4/3 cells in the presence or absence of parathyroid hormone (PTH; $10^{-8}M$). Osteoprotegerin (OPG; 100 ng/ml) was added to some cocultures treated with PTH. After 14 days, cells were fixed and stained for tartrate-resistant acid phosphatase (TRAP) or vitronectin receptor (VNR). Bar = 100 μm. **B,** NCD14+ monocytes and SaOS-4/3 cells were cocultured for 14 days with vehicle (control) (lane 1), PTH ($10^{-8}M$) (lane 2), and PTH ($10^{-8}M$) plus OPG (100 ng/ml) (lane 3). Total RNA was extracted from the cocultures, and the expression of mRNA for calcitonin receptor (CTR) and GAPDH was analyzed by reverse transcription–polymerase chain reaction.